MiR-1908 Is a Cholesterol Responsive MicroRNA Implicated In Cholesterol Regulation

Kaitlyn Beehler

Thesis submitted to the University of Ottawa in partial fulfillment of the requirements for the Master's degree in Biochemistry

Biochemistry, Microbiology and Immunology
Faculty of Medicine
University of Ottawa

Abstract

Leveraging miRNA-Seq data and the 1000 Genomes imputed genotypes, we identified rs174561-C as a strong miRQTL for circulating miRNA-1908-5p ($P=4.8x10^{-31}$) which has an inverse relationship with circulating LDL-C, fasting glucose and A1c. Here I investigated the molecular mechanism(s) linking miR1908-5p to cholesterol metabolism. First, by overexpression experiments in HuH-7 cells demonstrate that the presence of the C allele, associated with lower LDL-C levels, significantly increases miR-1908-5p by 2.15-fold relative to the T allele. Further experiments revealed that 72-hour cholesterol depletion increases miR-1908-5p expression (2.11-fold) whereas cholesterol loading decreases miR-1908-5p expression (0.69-fold). Differential miR-1908-5p expression was then used to profile genes involved in lipoprotein signaling and cholesterol metabolism using a PCR array to identify *LDLR* as a gene of interest. Although total RNA and protein expression of LDLR was unchanged in response to differential miR-1908-5p expression, the ratio of the mature form to the cleaved form of LDLR decreased following miR-1908-5p inhibition (0.85-fold) and conversely, increased with mimic treatment (1.63-fold). Cleavage of the mature LDLR is known to reduce cell surface affinity for LDL. These findings uncover a potential mechanism linking miR-1908-5p to lower LDL-cholesterol levels through reduced LDLR cleavage.

Acknowledgements

First, I would like to give a sincere thank you to my supervisor, Dr. Ruth McPherson, for the invaluable expertise, support, direction, and encouragement she gave me through my research project and thesis writing. Her passion for science is truly inspiring.

I would like to thank my thesis advisory committee members, Dr. Katey Rayner and Dr. Thomas Lagace, for the time they dedicated and their recommendations on the progress of my project. Their practical feedback allowed my project to reach completion in an organized and timely fashion. I would also like to thank Dr. Mireille Ouimet for publishing my BioRender images with her licence.

I must express my heartful gratitude to the members of the McPherson lab both past and present for fostering an extremely positive work environment that thrives on the success of others. I would like to extend a special thank you to Paulina Lau for her readiness to help me troubleshoot techniques, analyze data, or understand the literature. It has been such a pleasure to work with each one of you and I will never forget our lab lunches and fun lab outings!

Finally, I would like to send a big thank you to my parents, Allan and Angie, as well as my fiancé, Brad. Thank you for constantly being by my side and for celebrating the small victories with me. Your kindness, patience, and support through the stressful moments is what allowed me to get through my degree. I can’t say thank you enough!

Table of Contents

List of Abbreviations

ABCG5 /8	ATP-binding cassette subfamily G member 5 /8
ACAT1 /2	Acetyl-CoA acetyltransferase 1 /2
Acetyl-CoA	Acetyl-coenzyme A
AGO	Argonaute
AKR1C4	3α-hydroxysteroid dehydrogenase
AKR1D1	$\Delta^{4\text{-}3}$-oxosteroid-5β-reductase
Apo-B100	Apolipoprotein-B100
Apo-CII	Apolipoprotein-CII
Apo-E	Apolipoprotein-E
BMP1	Bone morphogenic protein-1
BSEP	Bile salt export pump
CAD	Coronary artery disease
CDCA	Chenodeoxycholic acid
CETP	Cholesteryl ester transfer protein
CVD	Cardiovascular disease
CYP27A1	Sterol 26-hydroxylase
CYP39A1	24-hydroxycholesterol 7α-hydroxylase
CYP7A1	Cytochrome P450 7A1
CYP7B1	Cytochrome P450 7B1
CYP8B1	7-alpha-hydroxycholest-4-en-3-one 12-alpha-hydroxylase
CYP46A1	Cholesterol 24-hydroxylase
DGCR8	DiGeorge syndrome critical region 8
DNA	Deoxyribonucleic acid
DNAJA4	DNAJ heat shock protein family member A4
eIF4A-I /II	Eukaryotic initiation factor-4A-I /II
eQTL	Expression quantitative trait loci
ER	Endoplasmic reticulum

E-boxes	Enhancer boxes
FADS1 /2	Fatty acid desaturase 1 /2
FBS	Fetal bovine serum
FGF-19	Fibroblast growth factor 19
FH	Familial hypercholesterolemia
GWAS	Genome-wide association study
HDL	High-density lipoprotein
HMG-CoA	3-Hydroxy-3-Methylglutaryl-Coenzyme A
HMGCR	3-Hydroxy-3-Methylglutaryl-Coenzyme A Reductase
HPRT1	Hypoxanthine Phosphoribosyltransferase 1
HSD3B7	3β-hydroxysteroid dehydrogenase type 7
IDL	Intermediate-density lipoprotein
INSIG	Insulin induced gene
LA	Linoleic acid
LB	Lysogeny broth
LC-PUFA	Long chain polyunsaturated fatty acids
LD	Linkage disequilibrium
LDL	Low-density lipoprotein
LDL-C	Low-density lipoprotein cholesterol
LDLR	Low-density lipoprotein receptor
LPDS	Lipoprotein deficient serum
LPL	Lipoprotein lipase
LDLRAP1	Low-density lipoprotein receptor associated protein 1
LRP-1 /8	Low-density lipoprotein receptor related protein 1 /8
MβCD	Methyl-β-cyclodextrin
MAF	Minor allele frequency
miRISC	miRNA-induced silencing complex
miRQTL	MicroRNA expression quantitative trait loci

miRSeq	MicroRNA sequencing
MRE	miRNA response element
NaOH	Sodium hydroxide
PBS	Phosphate buffered saline
PCSK9	Proprotein convertase subtilisin/kexin type-9
PPIA	Peptidylprolyl isomerase A
Pre-miRNA	Precursor microRNA
Pri-miRNA	Primary microRNA
qRT-PCR	Quantitative real-time polymerase chain reaction
RanGTP	Ras-related nuclear protein GTP
RNA	Ribonucleic acid
RNAPII	RNA polymerase II
RNU48	Small nucleolar RNA, C/D Box 48
S1P /S2P	Site-1 protease /Site-2 protease
SCAP	Sterol regulatory binding protein cleavage activating proteins
SD	Standard Deviation
siRNA	Small interfering RNA
SNP	Single nucleotide polymorphism
SOAT1 /2	Sterol O-acyltransferase 1 /2
SRE	Sterol response element
SREBF1a /1c /2	Sterol regulatory binding protein gene 1a /1c /2
SREBP1a /1c /2	Sterol regulatory binding protein 1a /1c /2
SRP14	Signal recognition particle 14
STARD3	Star related lipid transfer domain containing 3
UTR	Untranslated region
VLDL	Very-low-density lipoprotein

List of Figures

List of Tables

1. Introduction

1.1 Coronary Artery Disease

Cardiovascular disease (CVD) is the number one cause of death worldwide [1]. The most common form of CVD is coronary artery disease (CAD) which results in reduced blood flow and oxygen delivery to the heart [1]. The main process underlying CAD is atherosclerosis and it is considered a chronic state of inflammation in response to lipid retention [2].

Atherosclerosis is characterized by the thickening of the arterial walls and lesion development in the arterial intima [2]. As the lesions progress, there is greater narrowing of the arterial lumen causing restricted blood flow to the heart [2]. In some cases, complex lesions can be unstable and rupture causing thrombosis [2]. This can culminate in complete occlusion of an artery feeding the heart or brain resulting in a myocardial infarction or stroke [2].

There are many progressive steps involved in atherosclerosis beginning with fatty streaks and often ending with plaque rupture [3]. According to the Response-to-Retention Hypothesis, early atherogenesis is caused by subendothelial retention of apolipoprotein B100 (Apo-B100)-rich, pro-atherogenic lipoproteins in the arterial wall [3]. Low-density lipoprotein (LDL) is pro-atherogenic and its subendothelial accumulation results in fatty streak development which is often seen in the arteries of children and young adults [4]. Once retained in the artery wall, these lipoproteins become oxidized which allows for macrophage recognition by scavenger receptors

followed by macrophage uptake resulting in foam cell formation [3]. The prolonged inflammatory state induced by the foam cells causes vascular smooth muscle cell proliferation and migration into the arterial intima [5]. These vascular smooth muscle cells can then proliferate and take up lipoproteins, contributing to foam cell formation and further lipoprotein retention [3]. They can also synthesize extracellular matrix components that allow for the creation of a fibrous lesion cap that acts as a protective barrier to plaque rupture and thrombosis [6]. As the plaque grows, the arterial lumen narrows resulting in restricted blood flow which can cause chest pain or angina [7]. In some cases, the plaque can become unstable and vulnerable to rupture because of thinning of the fibrous cap, a large necrotic core, and a heightened inflammatory state [6]. Plaque rupture exposes the lipids and other components to blood components which initiates the coagulation cascade and thrombosis resulting in a coronary artery event [7].

There are many therapies being tested to prevent plaque formation and rupture in order to reduce the risk of cardiovascular events. One of the most robust CVD risk factors is an elevated level of circulating LDL-cholesterol (LDL-C) [5]. Atherosclerosis has been induced by increases in plasma LDL-C in every mammalian species ever studied [5]. This is why the most successful therapy for preventing coronary artery disease is lowering the amount of circulating LDL-C [8]. This therapy not only attenuates subendothelial lipoprotein retention, but also improves endothelial function and promotes the efflux of lipid-containing macrophages from the lesions [8]. Plaque progression is dependent on the levels of circulating LDL-C and a number of other cardiovascular risk factors: diabetes,

hypertension, obesity, or smoking [9]. All of these cardiovascular risk factors contribute to endothelial dysfunction which causes increased permeability to lipoproteins and other blood components [9]. So although other therapies that prevent LDL oxidation, or decrease inflammation, may be of benefit, they will be used in conjunction with therapies that lower circulating levels of pro-atherogenic lipoproteins [8].

1.2 Lipoprotein Transport and Cholesterol Metabolism

There are many different classes of circulating lipoproteins that can be distinguished as pro-atherogenic or anti-atherogenic based on their specific apolipoprotein profile and lipid composition. The 4 main types are: chylomicrons, very low-density lipoproteins (VLDL), low-density lipoproteins (LDL), and high-density lipoproteins (HDL) [10]. VLDL and LDL are pro-atherogenic lipoproteins, while HDL is considered anti-atherogenic [10]. Lipoproteins consist of a hydrophobic core that carries cholesterol in the form of cholesteryl esters and fatty acids in the form of triglycerides [5]. The hydrophobic core is surrounded by a polar phospholipid layer and specific apolipoproteins on the outer surface [5]. The major role of lipoproteins is to transport hydrophobic cholesterol and triglycerides to various tissues in the body [10].

Cholesterol is an essential molecule required to maintain the structure and function of all human cells. Cholesterol is located in the phospholipid bilayer in the spaces between the polar head groups and it is responsible for maintaining cell

membrane integrity and reducing membrane fluidity [11]. Cholesterol is also implicated in cell signalling and it is a precursor for the synthesis of bile acids, steroid hormones, and vitamin D [11]. Although cholesterol has many essential functions, insufficient or excessive levels of cholesterol in the bloodstream or in the cells has detrimental effects on the body [12]. For this reason, cholesterol homeostasis is very tightly regulated [12].

The liver accumulates cholesterol through either *de novo* cholesterol synthesis or through gut absorption of dietary cholesterol [5]. Hepatocytes have the ability to synthesize cholesterol from acetyl-Coenzyme A (acetyl-CoA) through a highly regulated process involving 3-hydroxy-3-methylglutaryl-coenzyme A (HMG-CoA) reductase (HMGCR) [12]. HMGCR is the rate-limiting enzyme in the intracellular cholesterol biosynthesis pathway in the endoplasmic reticulum (ER) and this enzyme is inhibited when cholesterol is present in the diet thereby shutting down *de* novo cholesterol synthesis [5]. Dietary lipids are emulsified and solubilized by bile acids in the intestine and taken up into enterocytes [13]. Enterocyte cholesterol can be secreted back into the lumen or it can be processed into chylomicrons or HDL particles [13]. Chylomicrons are large triglyceride-rich lipoproteins containing a core of cholesteryl esters that are released from the intestine into the circulation [10]. As the chylomicrons travel through the bloodstream, they acquire apolipoprotein CII (Apo-CII) and apolipoprotein E (Apo-E) from HDL particles [13]. When chylomicrons approach peripheral tissues like muscle and adipose tissue, Apo-CII interacts with lipoprotein lipase (LPL) and this causes most of the triglycerides to be hydrolyzed into free fatty acids [13]. The free fatty acids can then be taken up by the adipose or

muscle cells for energy production or storage or returned to the liver for *de novo* triglyceride synthesis [10]. Triglyceride hydrolysis results in a decrease in the size of the chylomicron particle and the formation of a cholesterol-rich chylomicron remnant [13]. The majority of the dietary cholesterol contained in the chylomicron remnants is delivered to the liver through interactions with hepatic receptors mediated by chylomicron remnant Apo-E [14]. Hepatic cholesterol and fatty acids can be used for VLDL assembly; cholesterol can be used for bile acid synthesis, or secreted back to the intestine [10].

The liver balances triglyceride uptake, synthesis and secretion to maintain triglyceride homeostasis [15]. Triglycerides can be derived through uptake of plasma lipoproteins or *de novo* hepatic lipogenesis from glucose, free fatty acids, and alcohol [15]. The liver secretes triglycerides in the form of triglyceride-rich lipoproteins, VLDL, or utilizes them in the form of fatty acid oxidation for energy [15]. The liver secretes cholesteryl esters, phospholipids, and triglycerides as VLDL particles that are released into the circulation [10]. These particles travel in the bloodstream and acquire Apo-CII from HDL particles very similarly to chylomicrons [13]. This allows for triglyceride hydrolysis by LPL and free fatty acid uptake by surrounding peripheral tissues [13]. Interactions between VLDL and HDL particles allows for the transfer of cholesteryl esters from HDL to VLDL through cholesteryl ester transfer protein (CETP) [10]. Through LPL and CETP the VLDL particles are converted into cholesterol-rich intermediate-density lipoproteins (IDL) [10]. IDL particles acquire Apo-E from HDL particles which allows them to circulate back to the liver for clearance via Apo-E receptors including the LDL receptor (LDLR), LDL Receptor Related

Protein 1 (LRP-1), or an Apo-E receptor [10]. The liver directly clears approximately 50% of IDLs and the remainder are further hydrolyzed by hepatic lipases to form cholesterol-rich LDL particles [5].

The majority of LDL is removed from the bloodstream through interactions of Apo-B100 with LDLR in the liver [5]. The discovery of LDLR came from the studies of familial hypercholesterolemia (FH) [5]. FH is caused by a single gene mutation that results in elevated plasma levels of LDL by approximately 2-fold [5]. Goldstein and Brown studied the regulation of cholesterol through the isolation of human cultured fibroblasts from normal subjects and patients with FH [5]. The cultured fibroblasts from healthy subjects were able to maintain cholesterol homeostasis through the uptake of LDL particles in the serum of the culture medium and through intracellular cholesterol synthesis [5]. They found that the fibroblasts originating from FH patients had an inability to uptake serum LDL particles [5]. These FH fibroblasts were still able to survive through increasing the expression of HMGCR by nearly 100-fold thereby promoting *de novo* intracellular cholesterol synthesis [5]. They discovered that the mechanism of cholesterol uptake from serum LDL was mediated through LDLR [5]. The FH defect is most commonly in the LDLR gene and depending on the type of mutation, some patients have either diminished LDLR activity (5-25% of normal) or complete dysfunction of LDLR [5]. LDLR deficiencies often result in atherosclerotic plaque progression due to the buildup of plasma LDL and prolonged circulation time which eventually leads to arterial deposition [5]. These studies highlight the importance of LDLR in the removal of excess LDL from the bloodstream and present a new area of research that could lead to new therapeutics for treating excess levels

of serum LDL. Less common causes of FH are mutations in the APOB gene that inhibit binding to the LDLR or a gain of function mutation in proprotein convertase subtilisin/kexin type-9 (PCSK9) [16].

At the cell surface of hepatocytes, LDLR associated protein 1 (LDLRAP1) interacts with the cytoplasmic tail of LDLR and it is important for the binding and catabolism of LDL-C, as well as LDLR recycling [16]. Following binding of circulating LDL to hepatic LDLR via Apo-B100, the receptor complex is internalized via clathrin-coated pits which fuse with early endosomes (**Figure 1**) [16]. In the endosome, the LDLR-LDL complex is exposed to an acidic environment that causes a conformational change in LDLR that promotes the release of LDLR from the complex [11]. The dissociated LDLR is then recycled back to the plasma membrane at the cell surface and this process can take place more than 100 times for a single receptor [16]. The non-recycled components of the endosome, mainly cholesteryl esters, are then delivered to lysosomes where the cholesteryl esters are hydrolyzed to free cholesterol and released into the bulk plasma membrane pool [17]. The process of LDLR recycling can be inhibited in the presence of PCSK9 [18]. PCSK9 is a secreted protein that is mainly synthesized in the liver under the control of the sterol regulatory binding protein-2 (SREBP-2) [18]. There are 2 main mechanisms by which PCSK9 targets LDLR for degradation: intracellular LDLR degradation and cell-surface LDLR degradation [18]. Intracellular PCSK9 can bind and redirect fully processed LDLR from the Golgi to the lysosome [18]. PCSK9 that has been secreted into the circulation can bind to LDLRs on the cell surface and once internalized, PCSK9 inhibits endocytic recycling which results in lysosomal degradation of both

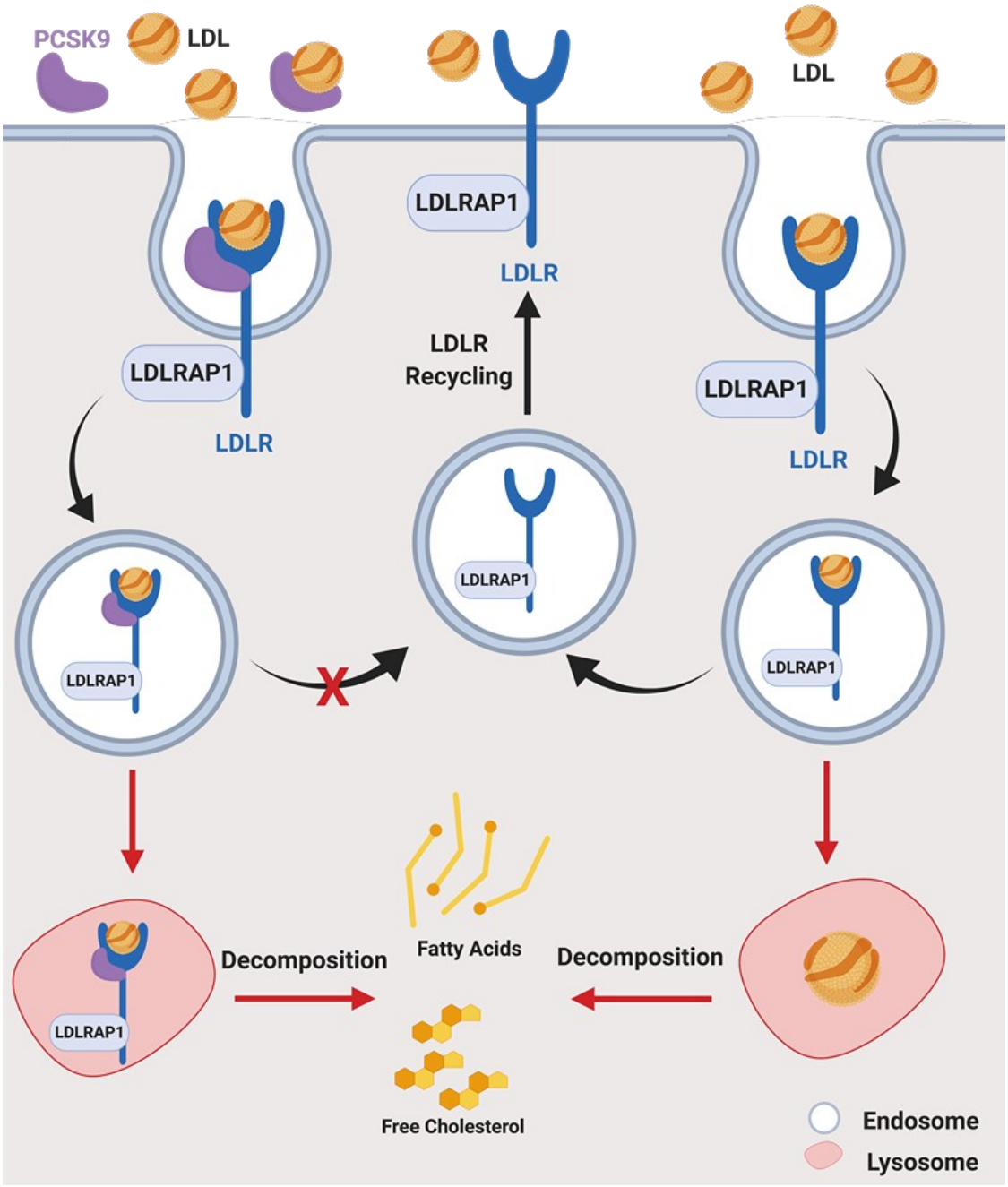

Figure 1. LDL-C clearance and recycling of LDLR.
At the cell surface of hepatocytes, LDLR interacts with LDL and initiates endocytosis. The acidic environment of the endosome induces a conformational change in LDLR that promotes its recycling back to the cell surface. The non-recycled component of the endosome undergoes lysosome degradation to release free fatty acids and free cholesterol. If PCSK9 binds to LDLR, the recycling pathway is inhibited and the whole PCSK9/LDLR complex get degraded in the lysosome. Image created with BioRender.com.

PCSK9 and LDLR [18].

The master transcriptional regulators of cholesterol and lipid homeostasis are SREBPs [19]. This transcription factor family consists of three members and each of them has a slightly different function. The *SREBF1* gene has two isoforms, SREBP-1a and 1c, which differ in their first exon due to alternate promoters of the gene [19]. SREBP-1a is expressed in highly proliferative cells and thus it activates both cholesterol synthesis and fatty acid synthesis to supply the major cell membrane components [20]. SREBP-1c is expressed mainly in the liver and it regulates the transcription of fatty acid synthesis genes in response to cellular insulin levels [19]. SREBP-1c is also responsible for the regulation of fatty acid desaturase 1 and 2 (FADS1 and FADS2) [21]. These genes are important for the conversion of dietary linoleic acid (LA) and α-linolenic acid (ALA) into long chain polyunsaturated fatty acids (LC-PUFA) [21]. VLDL formation in the liver is dependent on the conversion of these LC-PUFAs into phospholipids, triacylglycerols, or cholesteryl esters [21]. The last member of the SREBP family is SREBP-2 encoded by the *SREBF2* gene that is predominantly expressed in the liver [19]. SREBP-2 is the main transcriptional regulator of the cholesterol synthesis and cholesterol uptake pathways in hepatocytes [19].

Each of these SREBPs has 3 levels of regulation: transcriptional regulation, proteolytic cleavage of inactive precursors, and post-translational modification [20]. Each member of this transcription factor family is processed through the same general mechanism; however, there are key differences in their regulation [20]. SREBP-1a and SREBP-2 are mainly regulated through the proteolytic cleavage of

inactive precursors, while SREBP-1c relies heavily on transcriptional regulation [20]. SREBP-1c transcription is induced by insulin and this results in increased expression of the transcription factor in the nucleus as well as increased expression of the membrane-bound precursor in the ER [20]. Although SREBP-2 does not rely heavily on transcriptional regulation, transcription of *SREBF2* is induced under cholesterol-depletion conditions [20]. Following transcription of the *SREBF* genes, the mRNA is translated and the SREBP precursors bind to SREBP cleavage activating proteins (SCAP) in the ER membrane (**Figure 2**) [5]. When the intracellular levels of cholesterol increase, cholesterol binds to SCAP and induces a conformational change that results in the binding of insulin induced gene (INSIGs) proteins [5]. When the SCAP/SREBP complex is bound to INSIGs, SCAP is locked in a conformation that can no longer bind to COPII proteins which are required for the transportation of the complex to the Golgi apparatus for further processing [5]. Overall, the sequestering of the inactive SREBP precursor in the ER, leads to a decrease in transcription of the downstream target genes like HMGCR, LDLR, and PCSK9 [5]. When the hepatic levels of cholesterol decrease, the INSIG protein dissociates from the SCAP/SREBP complex [5]. This results in binding of the SCAP/SREBP complex to COPII proteins which allows for vesicular transport of the complex to the Golgi apparatus [5]. It is important to note that this process is dependent on insulin levels for SREBP-1c [20]. In the Golgi apparatus, the SREBPs are cleaved into their active forms and released by site-1 protease (S1P) and site-2 protease (S2P) [5]. The active form of these transcription factors binds to importin-β allowing for their translocation into the nucleus [20]. After entering the nucleus, these active SREBP transcription factors bind to the sterol response element (SRE) or enhancer boxes (E-boxes) in

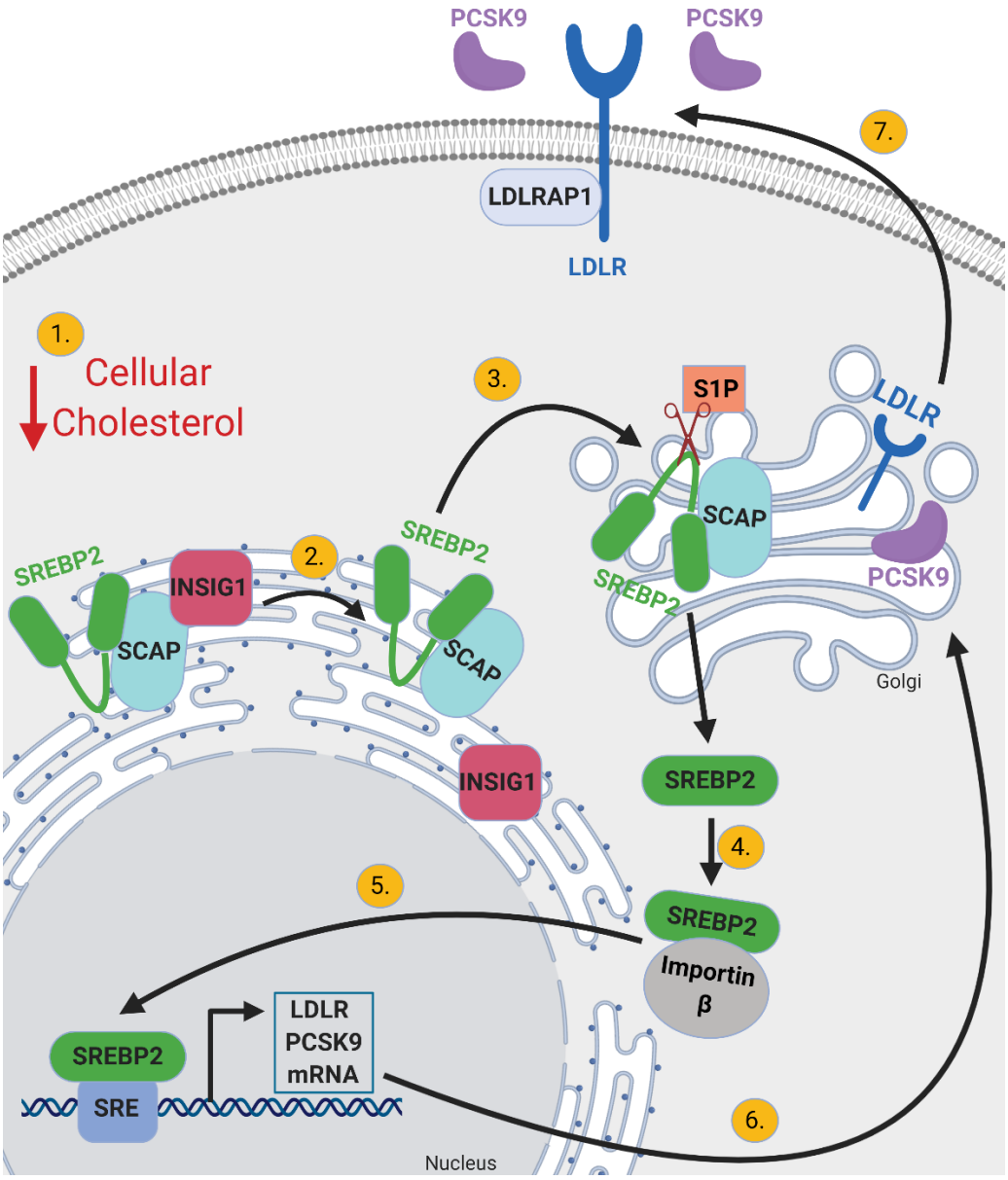

Figure 2. Transcriptional and posttranscriptional processing of LDLR and PSCK9.
(1) A decrease in hepatic cellular cholesterol causes (2) disassociation of INSIG1 from the SREBP2/SCAP complex. (3) The complex is transported to the golgi where S1P and S2P cleave SREBP2 into an active transcription factor that (4) associates with Importin β in the cytoplasm. (5) SREBP2 translocates into the nucleus where it binds to the SRE of its target genes, like LDLR and PCSK9, and upregulates their transcription. (6) After transcription and translation, the target proteins travel to the golgi for posttranslational modification. (7) Once in the mature form, LDLR associates with LDLRAP1 for its stable expression at the cell surface, and PCSK9 gets secreted into the bloodstream. Image created with BioRender.com.

the promoters of their target genes [20]. The transcriptional signal is terminated through the rapid degradation of SREBPs via the ubiquitin-dependent proteasome or through sumoylation which represses their transcriptional activities [20]. SREBP residue phosphorylation allows for E3 ubiquitin activating enzyme recognition that targets the protein for proteasomal degradation [22]. This degradation can be regulated through coactivator-mediated acetylation which increases the nuclear stability and the transcriptional activity of SREBPs [22]. Ultimately, the upregulation of the SREBP transcription factors lead to increased concentrations of hepatic free fatty acids and free cholesterol.

1.3 Bile Acid Synthesis

Free hepatic cholesterol can be delivered to the plasma membrane at the cell surface or to the endosomal plasma membrane via star related lipid transfer domain containing 3 (*STARD3*) [23]. It can also be esterified by acetyl-CoA acetyltransferase 1 and 2 (ACAT1 /2), encoded by sterol O-acyltransferase 1 and 2 (*SOAT1 /2*), and stored as lipid droplets in the ER [24]. Excessive accumulation of intracellular cholesterol is toxic to the cells and, therefore, it is crucial to sustain cholesterol homeostasis by getting rid of excess cholesterol. The major pathway that accounts for 90% of hepatic cholesterol catabolism and excretion is the conversion of cholesterol into bile acids [25]. Other minor routes for the elimination of cholesterol include: the conversion of cholesterol to steroid hormones, oxysterol production by the brain and lungs, or conversion into vitamin D [25]. Primary bile acids can be

synthesized via the classical pathway or the alternative pathway (**Figure 3**) [26]. The initiating and rate-limiting enzyme of the classical pathway is cytochrome P450 7A1 (CYP7A1) and it is responsible for the conversion of cholesterol into 7α-hydroxycholesterol [25]. The sterol ring is then further modified by 3β-hydroxysteroid dehydrogenase type 7 (HSD3B7) then the product of this can take two different routes depending on the activity of 7-alpha-hydroxycholest-4-en-3-one 12-alpha-hydroxylase (CYP8B1) [26]. For the formation of cholic acid, the intermediate will be hydroxylated by CYP8B1 at the C-12 position [27]. Absence of C-12 hydroxylation results in the formation of chenodeoxycholic acid (CDCA) [27]. Next, the intermediates are reduced by $\Delta^{4\text{-}3}$-oxosteroid-5β-reductase (AKR1D1) and 3α-hydroxysteroid dehydrogenase (AKR1C4) followed by side chain oxidation via sterol 26-hydroxylase (CYP27A1) [27]. The final step is peroxisome side-chain cleavage resulting in the formation of cholic acid and CDCA [28]. The ratio of cholic acid to CDCA, and thus the biological properties of the bile acid pool, is determined by the activity of CYP8B1 [26]. Primary bile acids can also be made from oxysterols via the alternative pathway [26].

Cholesterol 24-hydroxylase (CYP46A1) is responsible for the conversion of cholesterol in the brain into 24-hydroxycholesterol [27]. Studies show that 24-hydroxycholesterol and 25-hydroxcholesterol only contribute slightly to bile acid synthesis, while 27-hydroxycholesterol has a larger contribution [26]. The 7α-hydroxylation step of the alternative pathway for 24-hydroxycholesterol is performed by 24-hydroxycholesterol 7α-hydroxylase (CYP39A1), while 25- and 27-hydroxycholesterol is performed by cytochrome P450 7B1 (CYP7B1) [26]. These intermediates are then transported to the liver where they converge with enzymes

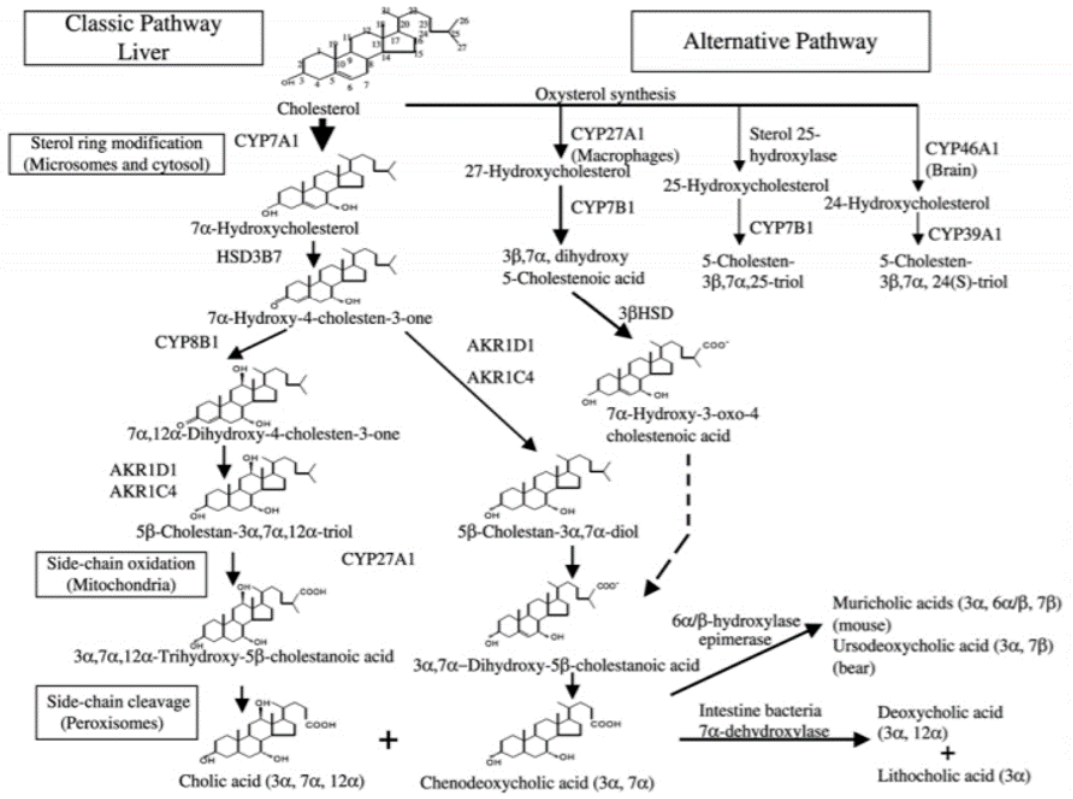

Figure 3. Pathways of bile acid synthesis.
The classical pathway is responsible for the synthesis of cholic acid and chenodeoxycholic acid (CDCA) from hepatic cholesterol. The alternative pathways are responsible for the transport and conversion of oxysterols from peripheral tissues to cholic acid and CDCA in the liver. Only the major enzyme and steps of each pathway is shown. Cholic acid and CDCA are conjugated and released into enterohepatic circulation where they can be deconjugated by intestinal bacteria into secondary bile acids like deoxycholic acid and lithocholic acid. Figure taken from John Y.L. Chiang, 2004, with permission [27]. License agreement number 4756800698202.

involved in the classic pathway to form cholic acid and CDCA [27].

Once bile acids are formed in the liver, they are conjugated to either glycine or taurine to increase their solubility for secretion into the bile along with phospholipids and sterols [27]. As the bile acids are transported into the canalicular space between hepatocytes, bile acid micelles can form allowing for uptake of cholesterol via ATP-binding cassette subfamily G member 5 (ABCG5)/G8 transporter [27]. The bile is secreted through intrahepatic bile ducts to the common bile duct and stored in the gallbladder until it receives a signal from the gut hormones to release the bile into the small intestine where they can emulsify and solubilize dietary cholesterol and lipids [25].

1.4 Genome Wide Association Studies and miRNA Sequencing

Coronary artery disease risk is influenced by both genetic and lifestyle factors [29]. Studies have shown that 40-50% of CAD susceptibility can be attributed to genetic variation [29]. Common genetic variants, also known as single nucleotide polymorphisms (SNPs), have a minor allele frequency of more than 1% of the population [30]. A SNP is a single nucleotide substitution at a specific position in the genome. SNP arrays that contain 200,000 to more than 2,000,000 SNPs across the genome can be used to compare a population of healthy individuals with a population of disease affected individuals to identify a genetic locus as a marker of disease susceptibility [30]. Using genome-wide association studies (GWAS), associations between the identified SNPs and various traits can be determined to

better understand the biology of the disease [30]. GWAS results have been published for hundreds of complex traits including common diseases, disease risk factors, gene expression, DNA methylation, and social traits [30]. GWAS currently relies on a concept called linkage disequilibrium (LD) which is the non-random association that exists between genetic variants in the human population due to evolutionary forces like natural selection and mutation/recombination rates [30]. One widely accepted conclusion from GWAS studies is that for any complex trait, there is always more than 1 loci contributing to the genetic variation [30]. This can be explained by the term polygenic which means that the disease risk for each individual is determined by the number of alleles that increase and the number of alleles that decrease the risk [30].

The experimental path from GWAS findings to biology is complicated because the association of a SNP with a trait does not provide any direct information for the target gene or the mechanism of how that genetic variant is associated with a difference in phenotype [30]. Pleiotropy also adds another layer of complexity because it disagrees with the “one gene, one function, one trait/disease” paradigm [30]. Pleiotropy is defined as one gene influencing two or more unrelated phenotypic traits [30]. New types of technology and analytical methods have been developed to bridge the gap between GWAS and molecular studies [30]. Between 2008 and 2015, the 1000 Genomes Project created the largest public database of genotype data and human variation [30]. Through the use of many publicly available databases that detail gene-mapping, tissue specific gene expression and epigenetics, GWAS has highlighted genetic variations associated with complex traits and diseases that have been further explained by basic research [30].

Identification of expression quantitative trait loci (eQTLs) is central to understanding complex diseases and thus integrating this data with GWAS can emphasize which genes to choose for functional follow-up studies to detect novel associations [30]. An eQTL is a genomic locus that explains part of the genetic variance observed in a phenotype [30]. Micro RNA (miRNA)-eQTLs (miRQTL) are an active area of research because they regulate the expression of miRNAs [31]. Due to the remarkable stability of miRNAs in the bloodstream, most studies have focussed on their potential as diagnostic biomarkers [31]. Our study was one of the first to use a multi-omics approach to study the relationships between SNPs, circulating miRNAs, intermediate molecular data, and phenotype [31]. MiRNA sequencing (miRSeq) was performed to profile 2083 circulatory miRNAs in 710 human subjects [31]. Leveraging the 1000 Genomes imputed genotypes and the miRSeq results, a GWAS study was performed to identify SNPs that regulate circulating miRNAs [31]. Mendelian randomization (MR) analysis identified miRQTLs involved in the regulation of intermediate molecular phenotypes in the blood [31]. GWAS significant SNPs were considered as mirQTLs based on a P<5E-8 [31]. miRSeq data set from the Geuvadis study was used for replication purposes to validate our findings [31]. We identified the rs174561-C SNP, intronic to the *FADS1* gene, that is associated with higher expression of miR-1908-5p (P_{mirQTL}= 4.8E-31). Rs174561 is a strong eQTL for *FADS1* in the liver (P_{eQTL}= 1.8E-6) and although it was not strongly associated with *FADS2* in the liver, it was indeed an eQTL for *FADS2* in many other tissues. Rs174561 is in tight LD with rs174548 (r2=0.97) and these results were consistent with the Geuvadis study [31]. Through SMR analysis, we found that higher expression of miR-1908-5p was associated with lower levels of circulating LDL (P_{SMR}= 2E-16),

total cholesterol (TC; P_{SMR}=4E-16), hemoglobin A1c (HbA1c; P_{SMR}= 6E-5), and fasting glucose (FG; P_{SMR}=2E-11) [31]. Further evidence showed that this effect was due to the regulatory effects of rs174548 on miR-1908-5p expression in the blood [31]. Although we did not measure the mature 3p-strand of miR-1908, data from the Geuvadis study showed a positive and significant association between rs174561-C and miR-1908-3p (P_{mirQTL}= 1.49E-08) [31]. Through the integration of various molecular and analytical methods, we identified miR-1908 as a miRQTL that is associated with circulating levels of TC, LDL, HbA1c, and FG [31].

1.5 miRNA Biogenesis and Mechanisms of Action

miRNAs are short non-coding RNAs of approximately 22 nucleotides that were first discovered in the early 1990s [32]. Some miRNAs are synthesized by the non-canonical pathway; however, the majority of miRNAs undergo canonical biogenesis (**Figure 4**). The first step of the canonical pathway is transcription of primary miRNAs (pri-miRNAs) which are either co- or post-transcribed with other RNA polymerase II (RNAPII) transcripts [33] . Of currently identified miRNAs, about half are processed from introns and the rest are synthesized independently of a host gene and have their own promoters [33]. Very few miRNAs are located in the exons of protein coding genes [33]. Pri-miRNAs can be composed of a cluster of related miRNAs, often with similar seed regions, or a single mature miRNA [33]. Pri-miRNAs are processed into precursor miRNAs (pre-miRNA) by a microprocessor complex that contains a DiGeorge Syndrome Critical Region 8 (DGCR8) protein, and Drosha

[33]. DGCR8 is an RNA binding protein that is responsible for recognizing a specific motif within the pri-miRNA structure [33]. Following recognition, Drosha is a ribonuclease III enzyme that cleaves the pri-miRNA at the base of the hairpin structure producing a pre-miRNA [33]. At the 3' end of the pre-miRNA, there is an overhang of 2 nucleotides that allows for recognition of the transcript by the exportin-5/RanGTP complex allowing for release of the pre-miRNA into the cytoplasm [33].

Following export, the terminal loop of the pre-miRNA is cleaved by the RNase III endonuclease, Dicer, resulting in the formation of a mature miRNA duplex [33]. The duplex contains a 5p strand that arises from the 5' end of the pre-miRNA and a 3p strand coming from the 3' end [33]. Using ATP, either of the mature miRNA strands can be loaded onto an Argonaute (AGO) protein but the proportion of the 3p vs 5p strand ranges from equal proportions to predominantly one or the other [33]. Typically, the strand with lower stability at the 5' end is preferentially loaded onto AGO and this is often dictated by cell type and cellular environment [33]. The strand that binds to AGO is the guide strand, while the other strand is called the passenger strand [33]. Humans express AGO protein 1-4 and while some miRNAs are loaded onto a specific AGO protein, most of them associate with all AGO proteins [32]. AGO2 is the most highly expressed and if the passenger strand has 100% sequence complementarity with the loaded guide strand, it will be cleaved by AGO2 and degraded [33]. If there are mismatches with the loaded guide strand or if the guide strand is loaded onto a non-AGO2 protein, the passenger strand is unwound and degraded [33]. miRNAs produced from the non-canonical pathway resemble canonical miRNAs structurally and functionally but they typically bypass a couple steps of the

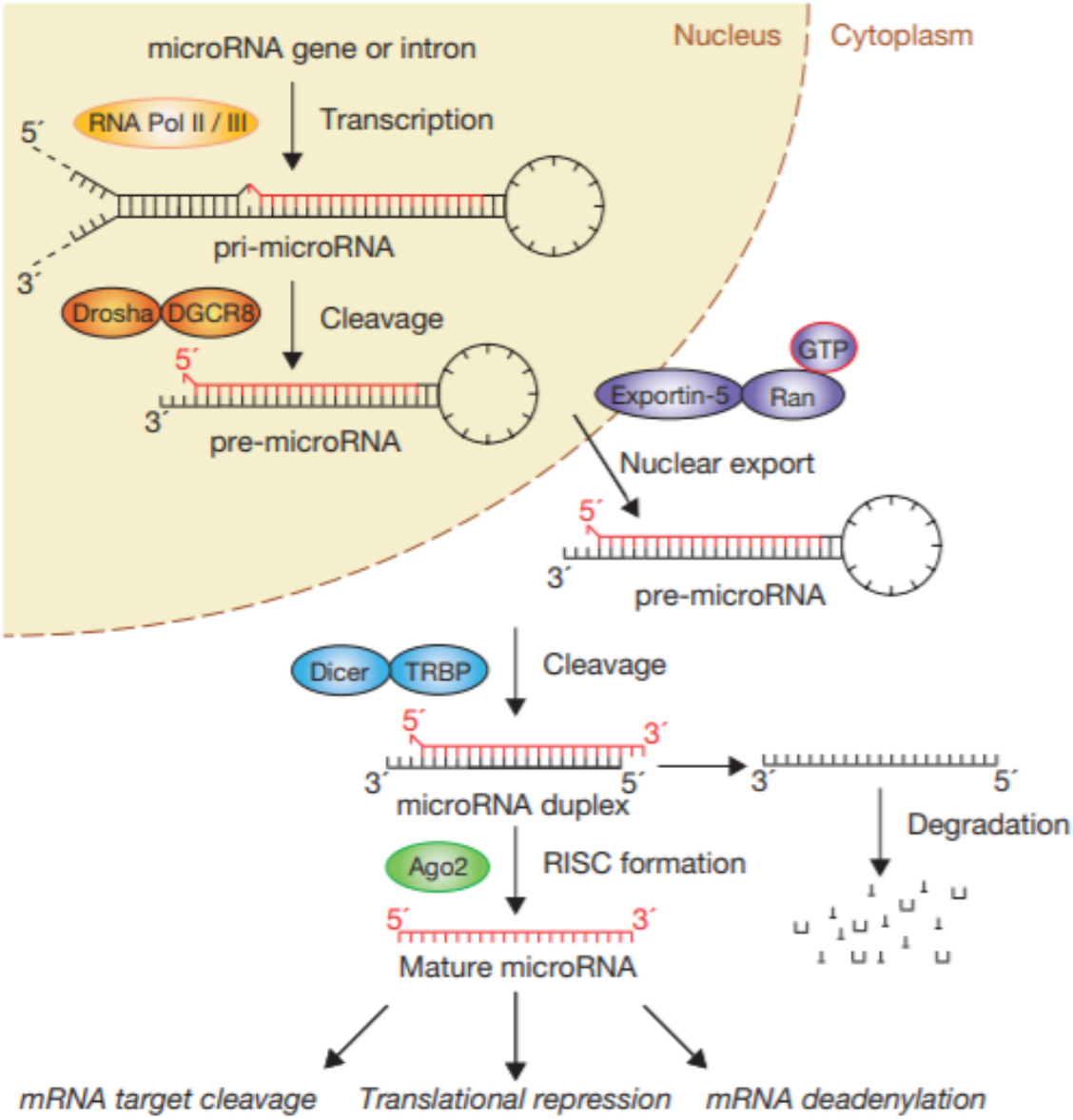

Figure 4. Canonical miRNA Biogenesis.
miRNA biogenesis begins with transcription of the primary miRNA (pri-miRNA) by RNA polymerase II/III. This transcript is cleaved by the Drosha/DGCR8 complex into precursor miRNA (pre-miRNA) which is then exported into the cytoplasm by Exportin-5-Ran-GTP. The pre-miRNA is cleaved by the Dicer/TRBP complex into a miRNA duplex structure. One strand from the miRNA duplex is loaded onto Ago2 forming the RNA induced silencing complex (RISC) which silences target mRNAs by cleavage, translational repression, or mRNA deadenylation. Figure taken from Winter *et al.,* 2009, with permission [34]. License agreement number 4756780087486.

dominant canonical pathway [33].

miRNAs mediate their effects on target messenger RNAs (mRNAs) through the minimal miRNA-induced silencing complex (miRISC) which consists of the guide strand, AGO, and other proteins [33]. The miRNA-loaded onto the AGO protein forms the targeting module of the miRISC [33]. Nucleotides 2-8 at the 5' end of the guide strand are known as the seed sequence and they are responsible for recognizing and binding to the target mRNAs [33]. The conformation of the miRISC allows for weak and rapid initial binding of the seed sequence to a miRNA response element (MRE) in the 3' untranslated region (UTR) of the target mRNA [32]. If the MRE presents sequence complementarity to nucleotides 7 and 8 of the seed sequence, then the interaction is stabilized and the AGO protein will remain engaged [32]. Nucleotides 13-16 of the miRNA, or the 3' half, are known as the supplemental region which can also help with target recognition [32]. The strongest MREs have an adenine opposite from the first nucleotide of the miRNA which is recognized by a binding pocket in the AGO protein [32]. AGO2-dependent cleavage of target mRNA is dependent on the level of MRE complementarity [33]. Target mRNA cleavage only occurs if the MRE is fully complementary with the miRNA and this causes destabilization resulting in degradation of the miRNA from the AGO complex [33]. Most of these interactions are not fully complementary in animals so AGO2 causes RNA interference which is similar to the action of AGO1, 3, and 4 [33]. Current evidence suggests that the miRISC represses translation of the target mRNA by functional interference of eiF4A-I/II and subsequent initiation of mRNA degradation

[35]. The miRISC mediates deadenylation of the poly-A tail which then promotes mRNA decapping rendering it susceptible to degradation by exoribonucleases [33].

In most cases, miRNAs tend to function in the cytoplasm by the mechanism described above, however, recent studies suggest that their activity can be modulated by nuclear localization or by extracellular vesicle transport [32]. Although most miRNAs bind to MREs in the 3' UTR of their target mRNAs, MRE sites have been detected in the 5' UTR, coding regions, and gene promoters of mRNAs [33]. These types of interactions have been reported to activate gene expression or translation of target mRNAs under specific conditions, however the mechanisms remain unclear [33]. Some studies suggest that nuclear miRNAs can regulate chromatin state or bind to complementary regions in the promoters of target genes thereby activating transcription [35]. miRNAs can also be secreted into extracellular fluids via vesicles or binding proteins like AGO allowing for miRNA-mediated cell-cell communication [33]. Atypical expression of miRNAs is often associated with human diseases and as such, extracellular miRNAs have been reported as potential biomarkers of disease due to their stability in the circulation [33].

1.6 The Role of miR-1908 in Human Disease

MiR-1908 was first discovered in 2008 in human embryonic stem cells [36]. The first functional study was performed in 2012 which focussed on melanoma metastasis and angiogenesis [37]. It showed that miR-199a-3p, miR-199a-5p, and miR-1908 synergistically repress APOE and DNAJ Heat Shock Protein Family

Member A4 (DNAJA4) [37]. DNAJA4 is responsible for upregulating the expression of APOE [37]. The combinatorial effect of these 3 miRNAs limits Apo-E secretion, thereby reducing the interaction of Apo-E with LRP-1 and LRP-8 [37]. This provides melanoma cells with high levels of invasion and endothelial cell recruitment leading to a poorer prognosis [37].

Since 2012, the cumulative work of many groups has shown differential expression of miR-1908 in many types of cancer. In most cases, the dysregulation of miR-1908 tends to promote cell proliferation, invasion, migration, and angiogenesis resulting in a decreased survival rate [38]. Many publications have highlighted its potential as a biomarker for predicting the survival rates of patients with certain kinds of cancer [39]. MiR-1908 has also been reported to be highly expressed in mature human adipocytes and may be involved in regulating the process of preadipocyte differentiation [40]. The expression of miR-1908 can be downregulated by free fatty acids and adipokines, like resistin and leptin, suggesting a role of miR-1908 in regulating obesity-related insulin resistance [41].

1.7 General Aims of Study

Leveraging miRNA-Seq data and the 1000 Genomes imputed genotypes, our lab identified a strong association of single nucleotide polymorphism rs174561 with increased plasma levels of miRNA-1908-5p [31]. A study by Ghanbari *et* al. showed that rs174561 in miR-1908 is associated with total cholesterol, LDL-cholesterol, HDL-cholesterol, triglycerides, and fasting glucose [42]. Since the SNP is located in the 5’ end of pre-miR-1908, they used the RNAfold predicted secondary structure of

miR-1908 to determine if this SNP has an effect on miRNA folding (**Figure 5**) [42]. They found that the rs174561-C allele had a lower minimum free energy than the more frequent U allele, meaning that it was more thermodynamically stable [42]. Bridging the gap, our lab further demonstrated an inverse relationship between circulating miR-1908-5p and blood levels of LDL, total cholesterol, fasting glucose, and hemoglobin A1c [31]. Here the molecular mechanism (s) linking miR-1908-5p to cholesterol metabolism has been investigated through the following specific aims:

Aim #1: Determine allele specific effects of rs174561 on miR-1908 expression.

Aim #2: Investigate the effect of cellular cholesterol on expression of miR-1908.

Aim #3: Determine the effect of differential miR-1908 expression on cellular cholesterol levels.

Aim #4: Identify target genes of miR-1908 relevant to cholesterol metabolism.

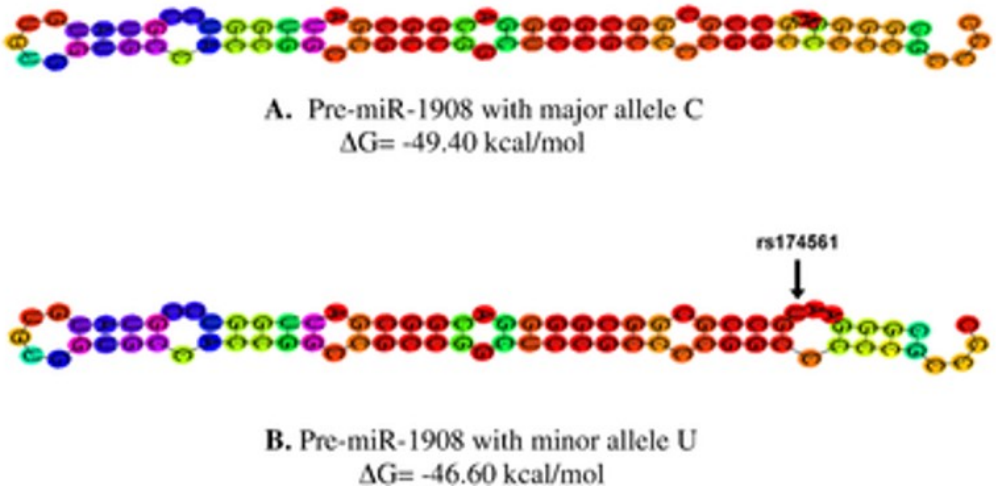

Figure 5. Schematic of the RNAfold predicted secondary structure of pre-miR-1908 with wild-type and mutant allele of rs174561.
(A) RNAfold predicted secondary structure with the C allele and the minimum free energy (ΔG). (B) RNAfold predicted secondary structure with the U allele. A lower MFE confers greater thermodynamic stability. Adapted from Ghanbari *et al*., 2014, with permission [42]. License agreement number 4730540971808

2. Materials and Methods

2.1 Cloning and Plasmid Preparation

The sequence of pri-miR-1908 containing either the A or G allele at the rs174561 SNP site was previously cloned into a pLVX vector in the laboratory by Paulina Lau (Lab Manager). NEB® 5-alpha High Efficiency Competent E. coli (NEB) expressing each of the plasmids above were stored at -80°C in 15% glycerol. An aliquot of each of these glycerol stocks was placed in a flask of LB containing 100µg/mL ampicillin (Roche) and these cultures were grown at 37°C overnight in an Orbital Shaker incubator (Forma Scientific) at 225rpm. The next day, plasmids were purified using the Plasmid Midi Kit (Qiagen) according the manufacturer's instructions and the concentration of DNA was measured using the NanoDrop-1000 Spectrophotometer.

2.2 Cell Culture Maintenance

Two hepatocellular carcinoma cell lines, HuH-7 and HepG2, were cultured in Dulbecco's Minimal Essential Medium containing 1g/L D-glucose, and supplemented with 10% Fetal Bovine Serum (Gibco), 1% L-Glutamine (Gibco), and 1% Penicillin-Streptomycin (Gibco). The cells were grown in a CO_2Water Jacketed Incubator (Forma Scientific) at 37°C with 5% CO_2 until they reached 90% confluency at which time they were passaged. Cells were lifted with 0.25% trypsin-EDTA solution (Gibco) for 5 mins at 37°C with 5% CO_2 then seeded into a new cell culture plate at a density that would reach 90% confluency when harvested or passaged again.

2.3 Pri-miR-1908 A vs. G Plasmid Treatment

HuH-7 cells were seeded for 24 hours then the cells were treated with 1µg of pri-miR-1908(T), pri-miR-1908(C), or empty pLVX plasmid using a Lipofectamine® RNAiMAX Reagent (Invitrogen) based transfection according to the manufacturer's instructions. The cells were harvested after 48 hours of treatment and quantitative real-time polymerase chain reaction (qRT-PCR) was used to measure the expression of miR-1908-3p and miR-1908-5p.

2.4 Cholesterol Depletion and Cholesterol Loading

One day after seeding, the HuH-7 cells were treated with either cholesterol depleted medium containing 10% LPDS (Gibco), 10 nM Rosuvastatin (Sigma), or both for 72 hours to cholesterol deplete the cells. Rosuvastatin was dissolved in DMSO at a concentration of 20mM prior to treatment. HuH-7 cells treated with medium containing 10% LPDS instead of 10% FBS were washed twice with 1X Phosphate Buffered Saline (PBS) before changing to medium containing 10% LPDS. 24 hours after seeding, HuH-7 cells were treated with 0.1 mM cholesterol-methyl-β-cyclodextrin (MβCD) (Sigma) for 24 hours to cholesterol load the cells. After harvest, the cells were stored dry at -20°C.

2.5 miR-1908-5p Inhibitor and Mimic Treatment

A hsa-miR-1908-5p miRIDIAN microRNA Hairpin Inhibitor, a miRIDIAN microRNA Hairpin Inhibitor Transfection Control with Dy547, a hsa-miR-1908-5p miRIDIAN microRNA Mimic, and a Mimic Transfection Control with Dy547 were purchased from Dharmacon and resuspended at a concentration of 50μM with water. The HuH-7 cells were seeded in 12-well plates at a density that would reach approximately 90% confluency at the point of harvest. After seeding, the cells were transfected with 9nM of the above reagents using Lipofectamine® RNAiMAX Reagent 24, 48, 72, or 96 hours. After harvest, the cells were stored dry at -20°C.

2.6 siRNA Treatment

Silencer Select Small interfering RNAs (siRNAs) were purchased from Thermo Fisher and resuspended at a concentration of 50μM with water. The HuH-7 cells were seeded and transfected with 20nM siRNA or negative control 1 using Lipofectamine® RNAiMAX Reagent for 48 hours. After harvest, the cells were stored dry at -20°C until the RNA and protein could be isolated.

2.7 Total RNA Isolation, cDNA Preparation, and Quantitative Real-Time PCR

After harvest, the cells were lysed with TriPure Isolation Reagent (Roche) for 10 min on an Adjustable Reciprocating Orbital Shaker (ThermoLyne). The total

RNA, including miRNA, was isolated from the samples using the Direct-zol RNA Miniprep Plus Kit (Zymo Research) according to the manufacturer's instructions. The on-column DNase digestion step of the Direct-zol RNA Miniprep Plus Kit was performed. The concentration of the RNA was determined using the NanoDrop-1000 Spectrophotometer.

500ng of total RNA was reverse transcribed using the Transcriptor First Strand cDNA Synthesis Kit (Roche) with oligo(dT) and random hexamer primers according to the manufacturer's instructions. The reaction was performed in a GeneAmp® PCR System 9700 (Applied BioSystems) then the samples were stored at -20°C. These cDNA samples were used to assess the relative mRNA expression of various genes using qRT-PCR (see **Table 1**. for primer sequences). The 20µL reaction was setup in a white LightCycler® 480 Multiwell Plate 96 (Roche) and contained 1X LightCycler® 480 SYBR® Green I Master Mix (Roche), 0.5µM forward primer, 0.5µM reverse primer, and 25ng of cDNA. QRT-PCR was performed using a touchdown program with the LightCycler® 480 I Instrument (Roche). The PCR products were verified by their melting curves and the fold change in mRNA expression was calculated using the ΔΔCt method with the reference genes: Hypoxanthine Phosphoribosyltransferase 1 (*HPRT1*) and Signal Recognition Particle 14 (*SRP14)*.

Total RNA (300ng) was used for cDNA preparation with the TaqMan™ MicroRNA Reverse Transcription Kit (Thermo Fisher Scientific) according to the manufacturer's instructions. This kit requires the use of specific TaqMan™ MicroRNA Assays which include a tube of specific reverse transcription primers and

Table 1. List of Genes and Primer Sequences for qRT-PCR.

Common Name	Gene Abbrevia-tion	Primer Direction	Sequence
Aldo-Keto Reductase Family 1 Member D1	*AKR1D1*	Forward	TGAACACGAAGTTGGGGAGG
		Reverse	CTAGCTGGAGGACCCTGAGT
Apolipoprotein E	*APOE*	Forward	CTGCGTTGCTGGTCACATTC
		Reverse	CGCAGGTAATCCCAAAAGC
Cytochrome P450 Family 7 Subfamily A Member 1	*CYP7A1*	Forward	AAGCAAACACCATTCCAGCG
		Reverse	GAACCGTCCTCAAGGTGCAA
Cytochrome P450 Family 7 Subfamily B Member 1	*CYP7B1*	Forward	TGCTGCAGTCAACAGGTCAA
		Reverse	GTCTCCCTTTCGCACACAGT
Cytochrome P450 Family 27 Subfamily A Member 1	*CYP27A1*	Forward	AGCGATACCTGGATGGTTGG
		Reverse	CTTTGAGCAACGGCATGTGG
Cytochrome P450 Family 39 Subfamily A Member 1	*CYP39A1*	Forward	GAGTATGGGTCCCAGTTGCC
		Reverse	CCCAAAGCAGTAAGAGCCCA
Fatty Acid Desaturase 1	*FADS1*	Forward	AGCTTTGAGCCCACCAAGAA
		Reverse	TTGAGGTGCTGAAGACCGAC
Fatty Acid Desaturase 2	*FADS2*	Forward	CTGGAGAGCCACTGGTTTGT
		Reverse	AGTAGCGGCTTCTCCTGGTA
Hypoxanthine Phosphoribosyltransferase 1 (Reference Gene)	*HPRT1*	Forward	TGCTGACCTGCTGGATTACA
		Reverse	GCCTGACCAAGGAAAGCAAAG
Insulin Induced Gene 1	*INSIG1*	Forward	CCTGGAGGAAACTCGGCAAT
		Reverse	TTCTGCTGACTGGTGGCTTC

Low Density Lipoprotein Receptor	*LDLR*	Forward	GCATGGGCCATTCTTCCTCT
		Reverse	TGGGTACGTGTGTCCAACAG
Low Density Lipoprotein Receptor Adaptor Protein 1	*LDLRAP1*	Forward	AGAAGAGGGACAAAGCCAGC
		Reverse	AACGCTTCATCCAGGCCATC
Proprotein Convertase Subtilisin/Kextin Type 9	*PCSK9*	Forward	GACGATGCCTGCCTCTACTC
		Reverse	CAGTCTCTGCCTCAACTCGG
Signal Recognition Particle 14 (Reference Gene)	*SRP14*	Forward	ACTTCCGGCTCTCACTGCTA
		Reverse	TCAAAGCCCTCCACAGTACC
Sterol Regulatory Element Binding Transcription Factor 2	*SREBF2*	Forward	GGGCTGGTTTGACTGGATGA
		Reverse	CCGGCACTGGAAGACTTTCT
StAR Related Lipid Transfer Domain Containing 3	*STARD3*	Forward	GATGGTATCTTGCCGCCCA
		Reverse	TCTTGCCGTGAAAGGGAACT

a tube of pre-formulated probe and primer mix for qRT-PCR (Thermo Fisher Scientific). TaqMan™ MicroRNA Assays were purchased for hsa-miR-1908-3p, hsa-miR-1908-5p, hsa-miR-16, and RNU48. The reaction was performed in the GeneAmp® PCR System 9700 (Applied BioSystems) then the samples were stored at -20°C. These cDNA samples were used to assess the relative microRNA expression using qRT-PCR. The 20µL reaction was setup in a white LightCycler® 480 Multiwell Plate 96 (Roche) and contained 1X TaqMan™ Fast Advanced Master Mix (Thermo Fisher Scientific), 1X pre-formulated assay (1 probe and 2 primers), and 30ng of cDNA. QRT-PCR was performed using the TaqMan™ MicroRNA Assay according to the manufacturer's instructions and the LightCycler® 480 I Instrument (Roche). The fold change in miRNA expression was calculated using the ΔΔCt method with the reference genes: hsa-miR-16 and RNU48.

2.8 Protein Isolation and Western Blots

The protein was isolated from the treated cells using RIPA buffer (150mM NaCl, 50mM Tris0HCl pH 8.0, 1% TritonX-100, 0.5% sodium deoxycholate, 0.1% SDS supplemented with 1x PhosSTOP (Roche) and 1x cOmplete™ Protease Inhibitor Cocktail (Roche)). Following 10 min of lysis at 4°C with gentle shaking, the cells were scraped and spun in the Sorvall Legend Micro 17 R Centifuge (Thermo Scientific) at 4°C for 15 min at 16,000xg to pellet the cell debris and the supernatant was collected and transferred to a new tube. The concentrations of the protein lysates were determined using a Pierce® BCA Protein Assay Kit (Thermo Fisher

Scientific) and a Synergy Mx microplate reader (BioTek) according to the manufacturer's instructions. The samples were stored at -20°C until use.

To prepare the samples for Western Blot, 3X SDS-PAGE loading buffer containing 15% β-mercaptoethanol was added to 20ug of the protein extract to a final concentration of 1X and 5% (v/v) respectively and the samples were boiled at 95°C for 5 min. The samples were then loaded onto a polyacrylamide gel, with a 4% stacking gel and an 8% running gel, alongside the Precision Plus Protein Ladder (BioRad). Gel electrophoresis was conducted at 200V until the dye-front reached the bottom of the gel. The gel was then transferred to a 0.45µm nitrocellulose membrane (BioRad) using a semi-dry transfer method or a wet transfer method. The semi-dry transfer method used the Trans-Blot® Turbo™ transfer system (BioRad) set at 25 limit volts, 2.5 constant amps, for 7 mins. The wet transfer method was performed in a chilled chamber containing 1X wet transfer buffer (25mM Tris Base, 192nM glycine) with 20% methanol and the gel was transferred overnight at 30V. Following the transfer, the membrane was blocked using 1:1 H2O: Odyssey Blocking Buffer, PBS (LI-COR® Biosciences) with gentle shaking for one hour at room temperature. Following blocking, the membrane was washed with 1X PBST or 1X TBST (depending on the primary antibody conditions) followed by overnight incubation of primary antibodies at 4°C (see **Table 2.** for primary antibody information). The monoclonal 15A6 PCSK9 antibody was a gift to our laboratory from Thomas Lagace at the University of Ottawa Heart Institute, Ottawa, ON. After overnight incubation, the primary antibodies were removed and the membrane was washed 3 times with 1X PBST or 1X TBST for 5 min. Secondary infrared dye

Table 2. Primary Antibody Specifications

Antibody	Company	Catalog Number	Dilution	Buffer Conditions
AKR1D1	Atlas Antibodies	HPA057002	1:1000	TBST
APOE	Millipore	AB947	1:1000	TBST
Beta Tubulin	GeneTex	GTX11307	1:1000	PBST
CYP27A1	Thermo Fisher Scientific	PA5-27946	1:1000	PBST
CYP39A1	Novus Bio	NBP2-50206	1:500	TBST
CYP39A1	Thermo Fisher Scientific	PA5-38909	1:1000	PBST
FADS1	GeneTex	GTX114528	1:1000	TBST
FADS2	GeneTex	GTX64748	1:1000	TBST
INSIG1	Novus Bio	NB110-55244SS	1:500	PBST
INSIG1	Abcam	Ab70784	1:500	PBST
LDLR	R&D	AF2148-SP	1:1000	PBST
PCSK9 (15A6)	Thomas Lagace's laboratory	-	10 µg/mL	PBST
SREBP2	Novus Bio	NB100-74543	1:500	PBST

(IRDye800)- labelled antibodies were purchased from LI-COR Biosciences. The membrane was incubated in the dark at room temperature with the proper secondary antibody at a dilution of 1:20,000 with the PBST or TBST. After 1 hour, the secondary antibodies were removed and the membrane was washed 3 times with 1X PBST or TBST for 5 min. Before scanning the membrane on a LI-COR Odyssey infrared imaging system (LI-COR Biosciences), the membrane was washed once with 1X PBS or 1X TBS without tween. The western blot scans were analyzed and quantified using Image Studio Lite Version 5.2 and the signal for the protein of interest was normalized to the signal of the beta tubulin loading control.

2.9 Lipid Isolation and Cholesterol Quantification

The lipids were harvested from the cells using a 7:11:0.1 chloroform:isopropanol:IGEPAL mixture with gentle shaking for 10 min. The samples were collected and centrifuged at 13,000 xg for 10 minutes to remove the insoluble material. The supernatant was transferred to a new tube and the organic solvent was evaporated using nitrogen spray. The dried lipids were dissolved in the Cholesterol Assay Buffer provided by the Amplex® Red Cholesterol Assay Kit (Thermo Fisher Scientific).

After the lipids were harvested, the remaining cell sample was lysed with 0.1 M NaOH for 10 minutes with gentle shaking. The samples were collected and centrifuged at 13,000 xg for 10 min to remove any cell debris. The supernatant was

collected and the samples were stored at -20°C until use. The protein concentrations were determined using the Pierce® BCA Protein Assay Kit.

All the Amplex® Red Cholesterol Assay Kit reagents were prepared according to the manufacturer's instructions prior to use. Once the standard curve was prepared for the assay, the dissolved lipids were diluted with cholesterol assay buffer to a suitable range within the standard curve and loaded into a black 96 well flat bottom assay plate (Corning). The reaction mixture was prepared and added to each of the microplate wells containing the standard curve and the samples according to the manufacturer's instructions. To measure the concentration of free cholesterol, cholesterol esterase was omitted from the reaction mixture. The microplate was incubated in a Dry Type Bacteriological Incubator (Fisher Scientific) in the dark at 37°C for 30 min. The fluorescence was measured using a SynergyMx microplate reader (BioTek) using an excitation of 545 ± 13.5 and an emission detection of 590 ± 9. The concentration of cholesterol was determined for each of the samples using the standard curve with known cholesterol concentrations. The calculated cholesterol concentrations were normalized to protein concentration of each sample.

2.10 Statistical Analysis

All data are reported as means ± standard deviation and statistical significance was determined using a 2-tail Student's t-Test.

3. Results

3.1 rs174561-C results in higher expression of miR-1908-5p

Our laboratory has demonstrated that rs174561-C is associated with higher expression of circulating miR-1908-5p [31]. To determine if rs174561-C is also a miRQTL in a hepatocyte cell line, HuH-7 cells, the sequence of pri-miR-1908 containing either the C or T allele at rs174561 was cloned into a pLVX vector. The plasmids were transfected into HuH-7 cells for 48 hours to overexpress the miRNA harboring either the T or C allele. The levels of miR-1908-3p and miR-1908-5p were measured using qRT-PCR and the fold change ratio of the C allele to the T allele was calculated using the puromycin resistance gene for normalization (**Figure 6**). As shown, the presence of the C allele does not change the expression of miR-1908-3p; however, the expression of miR-1908-5p is increased by 1.5-fold relative to the T allele.

3.2 miR-1908-5p expression is associated with cellular cholesterol

Previous bioinformatic studies in our laboratory also identified an inverse relationship between circulating miR-1908-5p and blood levels of LDL-C and total cholesterol suggesting that miR-1908 may be responsive to cholesterol levels [4]. To investigate the effect of cellular cholesterol levels on miR-1908 expression, HuH-7 cells were incubated in cholesterol depleted medium, or treated with rosuvastatin, or both for 72 hours. Rosuvastatin inhibits HMG-CoA reductase to deplete cellular cholesterol levels. HuH-7 cells are normally grown in medium containing 10% fetal

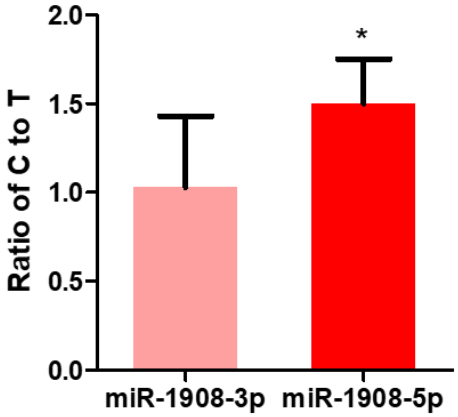

Figure 6. Presence of the C allele for rs174561 significantly increases miR-1908-5p by 1.50-fold relative to the T allele.
HuH-7 cells were treated with 1 µg of PLVX-Pri-miR-1908 (T or C) for 48 hours. The RNA was harvested and qRT-PCR was used to measure the expression of miR-1908-3p and miR-1908-5p. The ratio of C to T was calculated as the fold change in miR-1908 relative to the puromycin resistance gene using miR-16 and RNU48 for normalization. N=3. The error bars depict the SD. *p<0.05.

bovine serum (FBS), and replacement medium containing 10% lipoprotein deficient serum (LPDS) minimizes exogenous cholesterol supply. To maximally deplete cellular cholesterol, both interventions were combined. HuH-7 cells treated with 10% LPDS showed a 19% decrease in total cholesterol levels and a significant 1.60-fold increase in miR-1908-5p expression and a trend towards an increase in miR-1908-3p expression (**Supplementary Figure 1**). Rosuvastatin treated HuH-7 cells, in 10% FBS medium, exhibited a 58% decrease in total cholesterol and a significant 1.34- and 2.11-fold increase in miR-1908-3p and miR-1908-5p expression respectively (**Figure 7**). A 65% decrease in total cholesterol levels was observed in cells treated with rosuvastatin in 10% LPDS medium (**Figure 7A**). These cells had a 1.46-fold increase in miR-1908-5p expression and a trend towards an increase in miR-1908-3p expression (**Figure 7B and Figure 7C**). These data demonstrate that miR-1908-5p expression increases in a hepatocyte cell line in response to cholesterol depletion.

To further study the dependence of miR-1908 expression on cellular cholesterol, HuH-7 cells were treated with either rosuvastatin (cholesterol depletion) or with cholesterol loaded methyl-β-cyclodextrin (MβCD). The cells could be cholesterol loaded for only 24 hours as detrimental effects were seen after 72 hours of treatment due to the known toxicity of MβCD. After cholesterol loading or depletion treatment, the cells were harvested and the expression of miR-1908 was quantified by qRT-PCR. The fold change was calculated relative to the untreated cells using miR-16 and RNU48 for normalization. Rosuvastatin treatment resulted in a 0.55-fold decrease in total cholesterol and a significant 1.48-fold increase in miR-

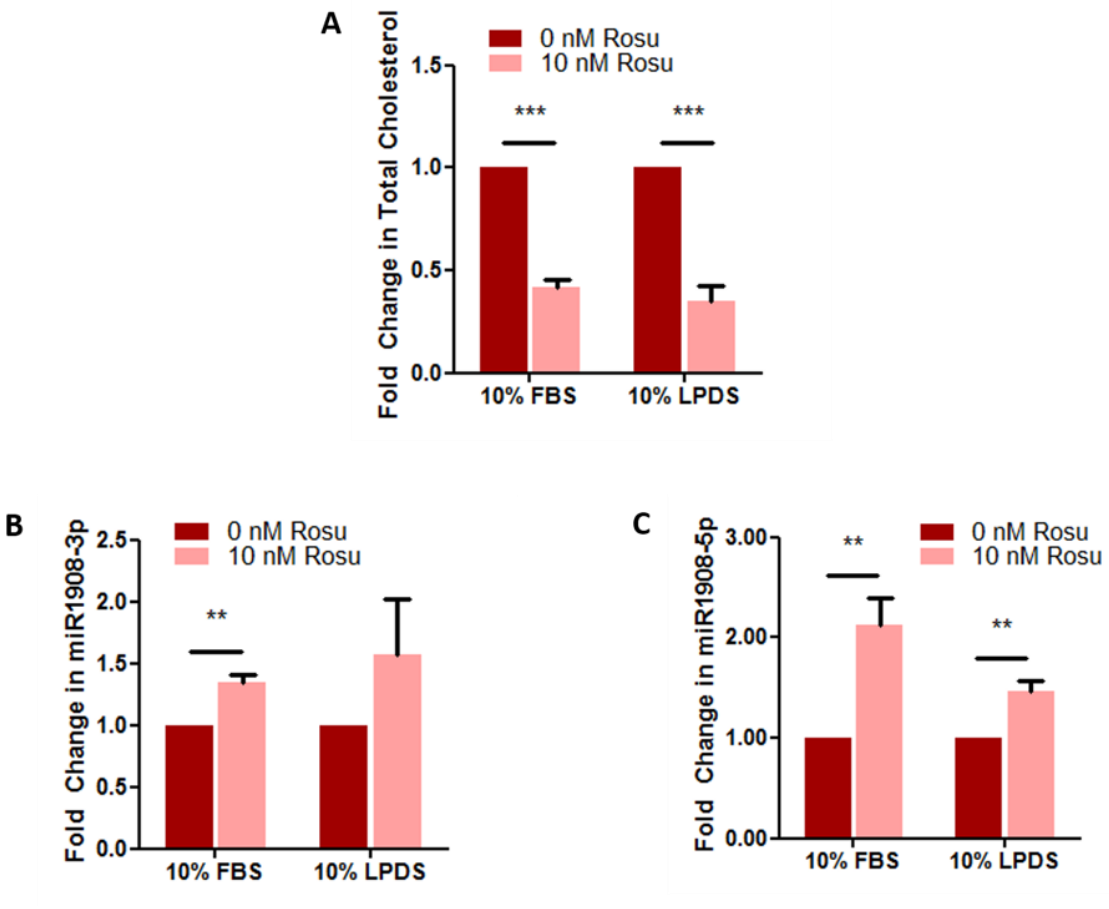

Figure 7. miR-1908 expression is increased under all cholesterol depletion conditions.
HuH-7 cells were treated with 10 nM rosuvastatin (Rosu) in medium containing 10% FBS or 10% LPDS. After 72 hours, the lipids and RNA were extracted from the cells. (A) The total cholesterol concentration, normalized to protein concentration, was calculated relative to untreated cells in 10% FBS or 10% LPDS using the Amplex Red Cholesterol Assay Kit. QRT-PCR was performed to measure the fold change in (B) miR-1908-3p or (C) miR-1908-5p relative to untreated cells, using miR-16 and RNU48 for normalization. N=4. The error bars depict the SD. **p<0.01, ***p<0.001.

1908-5p expression (no change in miR-1908-3p expression) (**Figure 8**).

HuH-7 cells treated with MβCD-cholesterol showed a significant 3.05-fold increase in total cholesterol (**Figure 8A**). Cholesterol loading resulted in a 0.69-fold decrease in miR-1908-5p expression and a change to a bias of increase in miR-1908-3p expression (**Figure 8B**). These findings reinforce the dependence of miR-1908 expression on cellular cholesterol levels.

3.3 miR-1908-5p has a role in cholesterol esterification

The demonstration that miR-1908-5p is associated with cellular cholesterol levels prompted the question: can miR-1908 regulate cellular cholesterol levels? miR-1908-5p was inhibited in HuH-7 cells using a hairpin inhibitor or a non-target transfection control. The samples were isolated after 24-96 hours of transfection and qRT-PCR showed reduction of miR-1908-5p by more than 80% (**Supplementary Figure 2**). A mimic targeting miR-1908-5p was also transfected into HuH-7 cells and it showed more than a 1000-fold increase in miR-1908-5p expression across various time points relative to the transfection control (**Supplementary Figure 2**). To assess whether miR-1908-5p regulates cellular cholesterol levels, HuH-7 cells were treated with inhibitor or mimic for 72 hours and cellular lipids were harvested. Cellular concentrations of free cholesterol, cholesteryl esters, and total cholesterol were determined and normalized to protein concentration. The level of total cholesterol and free cholesterol were not affected by differential miR-1908-5p expression(**Figure 9**). The cholesteryl esters in HuH-7 cells treated with the inhibitor

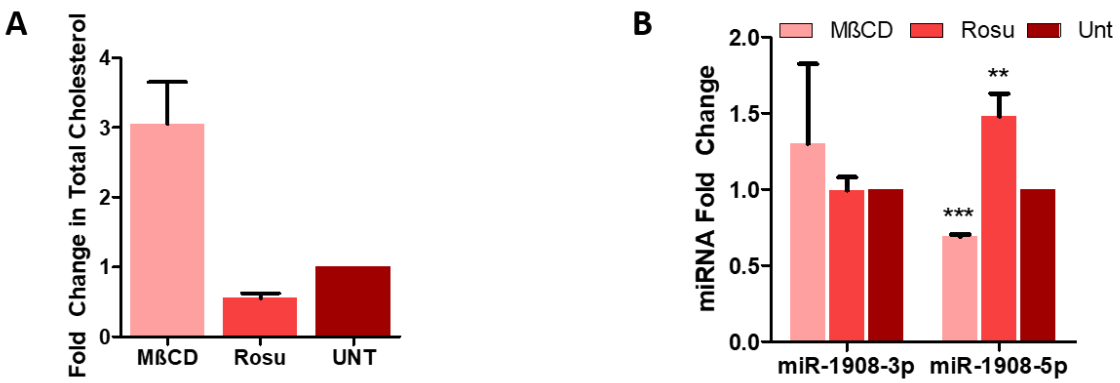

Figure 8. miR-1908-5p expression is associated with the levels of cellular cholesterol.

HuH-7 cells were treated with 0.1mM cholesterol-methyl-β-cyclodextrin (MβCD) or 10 nM rosuvastatin (Rosu) in medium containing 10% FBS. After 24 hours, the lipids and RNA were extracted from the cells. (A) The total cholesterol concentration, normalized to protein concentration, was calculated relative to untreated (UNT) using the Amplex Red Cholesterol Assay Kit. (B) QRT-PCR was performed to measure the fold change in miR-1908 expression relative to the untreated cells using miR-16 and RNU48 for normalization ± SD. N=3. **p<0.01 ***p<0.001.

showed a trend towards an increase, whereas mimic treatment decreased cholesteryl esters. These data indicate that miR-1908-5p may have a role in cholesterol esterification but further studies are required to validate this finding.

3.4 APOE, FADS1, and FADS2 expression remains unchanged with differential miR-1908-5p expression

Next, we turned our attention to the identification of miR-1908-5p targets. A previous study in the cancer field reported an inverse relationship between miR-1908-5p and APOE in mice [14]. To investigate this finding in liver, HuH-7 cells were treated with an inhibitor or mimic targeting miR-1908-5p. RNA expression was measured using qRT-PCR and the values were normalized to peptidylprolyl isomerase A (*PPIA*). The APOE protein expression was also measured and the values were normalized to the Beta tubulin loading control. The RNA expression of APOE had a very slight inverse correlation with the expression of miR-1908-5p, while the protein expression remained unchanged with inhibitor and mimic treatment (**Figure 10**). These data suggest that APOE is not highly regulated by miR-1908-5p in HuH-7 cells.

MiR-1908-5p is intronic to the FADS1 locus causing us to question whether FADS1 and FADS2, are affected by differential miR-1908-5p expression. HuH-7 cells were treated as described above. Differential miR-1908-5p expression did not change the RNA or protein expression of FADS1 or FADS2 (**Figure 11 and Figure 12)**. A FADS2 Human Over-expression Lysate was used as a positive control for the

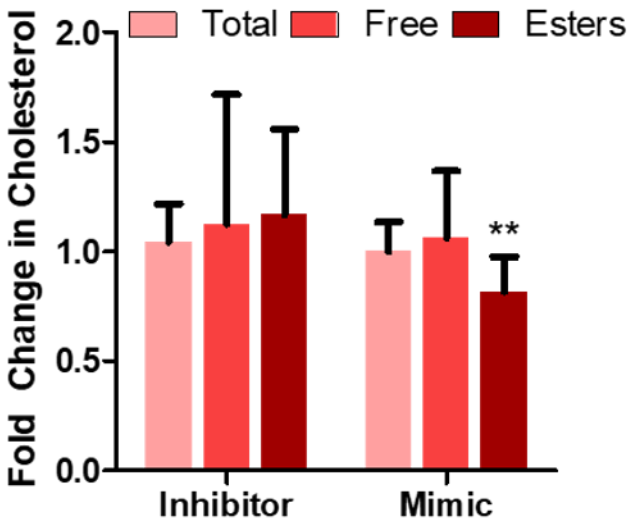

Figure 9. Differential miR-1908-5p expression does not affect total cholesterol levels.
HuH-7 cells were treated with 9 nM of miR-1908-5p inhibitor, mimic, or transfection control. After 72 hours of treatment, the lipids and protein were harvested from the cells. The concentration of total cholesterol and free cholesterol was measured using the Amplex Red Cholesterol Assay Kit and the concentration of cholesteryl esters was calculated as the difference of total and free cholesterol. The fold change in cholesterol was calculated as treatment relative to the transfection control, using protein concentration for normalization. N=8. The error bars depict the SD. **p<0.01.

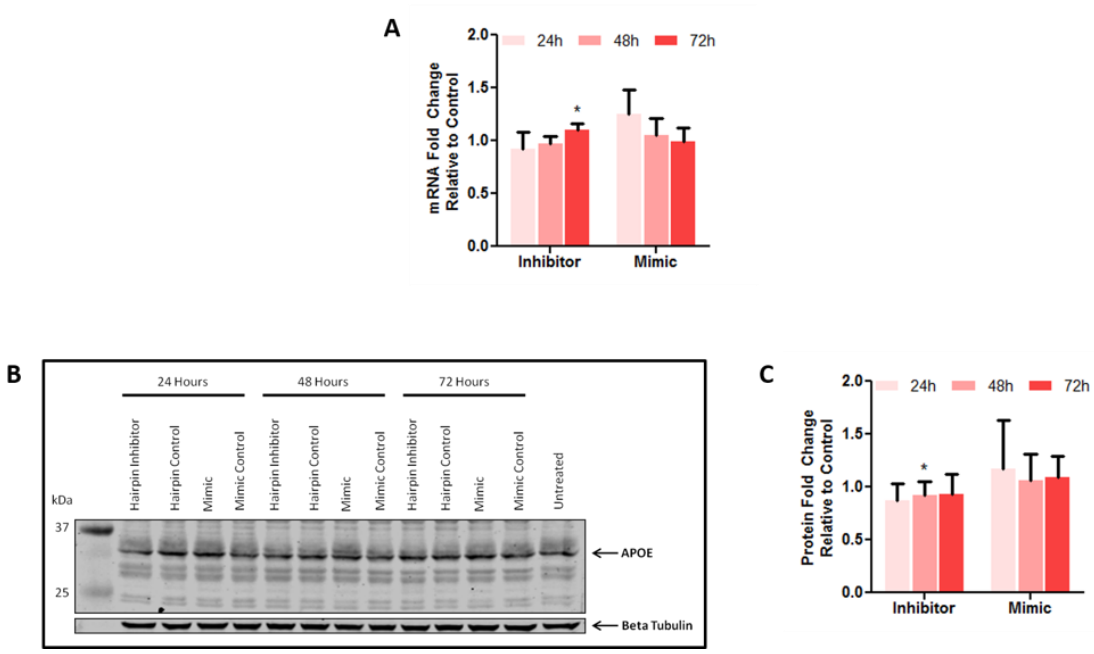

Figure 10. APOE expression remains unchanged with differential miR-1908-5p expression.

HuH-7 cells were treated with 9 nM of miR-1908-5p inhibitor, mimic, or transfection control. (A) *APOE* mRNA expression was analyzed using qRT-PCR. The mean fold change was calculated relative to the transfection control using *PPIA* for normalization for 3 independent experiments. (B) A Western blot was performed using Beta tubulin as a loading control to measure (C) the mean fold change in APOE protein expression relative to the transfection control for 3 independent experiments. Error bars depict the SD. *p<0.05.

FADS2 western blot (**Supplementary Figure 3**). Although rs174561 is a strong eQTL for *FADS1* in the liver, these findings demonstrate that there is no evident effect of miR-1908-5p on *FADS1* expression. These results also show that *FADS2* expression in the liver is not altered by miR-1908-5p, as predicted since rs174561 is not a reported eQTL for the *FADS2* locus in the liver.

3.5 Identification of potential target genes of miR-1908-5p

To find potential signaling pathways that respond to miR-1908-5p, HuH-7 cells were treated for 48 hours with inhibitor, mimic, or transfection control and were applied to a Cignal 45-Pathway Reporter Array. After 24 hours, a luciferase assay was performed and the values were normalized to the constitutively expressed Renilla construct. The fold change in pathway-specific transcription factor activity was calculated relative to the transfection control. Inhibition of miR-1908-5p caused an increase in *HIF1A* encoding the HIF-1α transcription factor that regulates the hypoxia signaling pathway; however, the mimic treatment also showed a trend towards an increase (**Figure 13A**). A significant decrease in *TGFB1* encoding TGF-β was also observed with mimic treatment (**Figure 13B**). Given the inconsistency in the Cignal Finder data between the inhibitor and mimic treatments, these findings are inconclusive. To search for targets of miR-1908-5p related to cholesterol metabolism, HuH-7 cells were treated with inhibitor or mimic for 48 hours and the RNA was applied a Lipoprotein Signaling and Cholesterol Metabolism RT2 Profiler PCR array (**Table 3**).

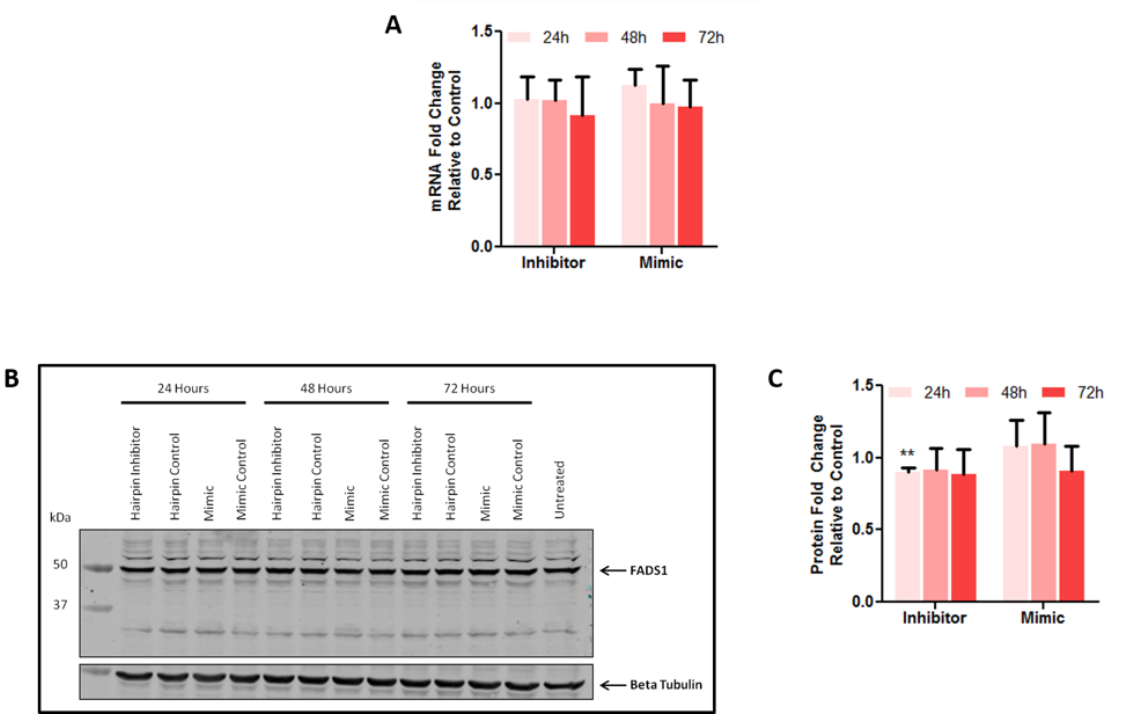

Figure 11. FADS1 expression remains unchanged with differential miR-1908-5p expression.

HuH-7 cells were treated with 9 nM of miR-1908-5p inhibitor, mimic, or transfection control. (A) *FADS1* mRNA expression was analyzed using qRT-PCR. The mean fold change was calculated relative to the transfection control using *PPIA* for normalization for 3 independent experiments. (B) A Western blot was performed using Beta tubulin as a loading control to measure (C) the mean fold change in FADS1 protein expression relative to the transfection control for 3 independent experiments. Error bars depict the SD. **p<0.01.

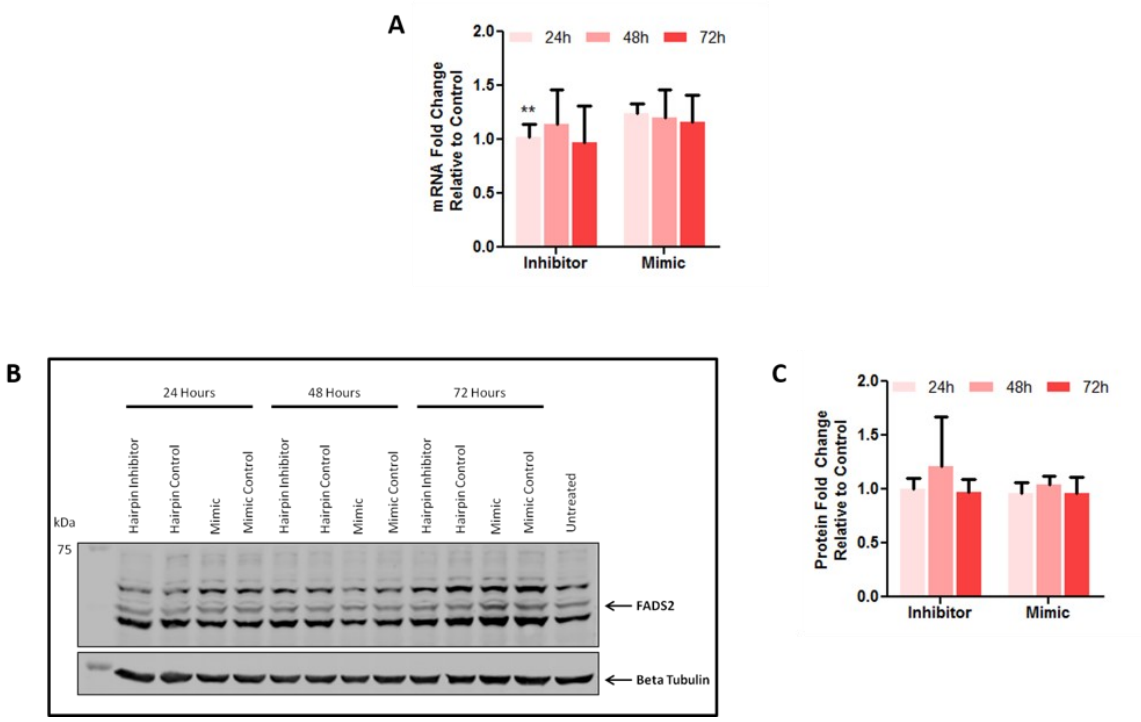

Figure 12. FADS2 expression remains unchanged with differential miR-1908-5p expression.

HuH-7 cells were treated with 9 nM of miR-1908-5p inhibitor, mimic, or transfection control. (A) *FADS2* mRNA expression was analyzed using qRT-PCR. The mean fold change was calculated relative to the transfection control using *PPIA* for normalization for 3 independent experiments. (B) A Western blot was performed using Beta tubulin as a loading control to measure (C) the mean fold change in FADS2 protein expression relative to the transfection control for 3 independent experiments. Error bars depict the SD. **p<0.01.

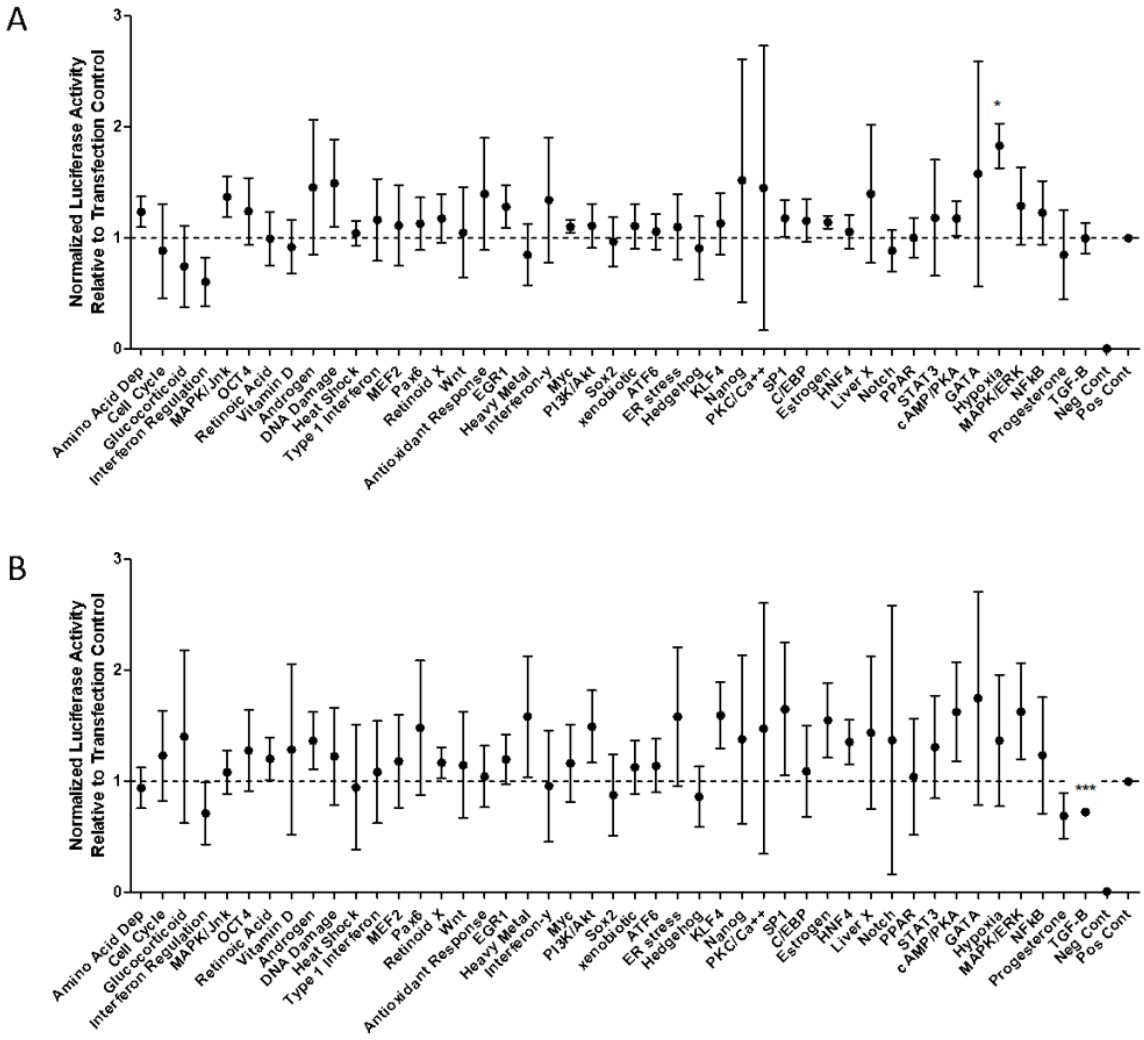

Figure 13. Differential miR-1908-5p expression affects the hypoxia and TGF-β pathways.

HuH-7 cells were treated with a miR-1908-5p inhibitor (A), mimic (B), or transfection control for 24 hours. Following treatment, the cells were reverse transfected into the Cignal 45-Pathway Reporter Array plates for an additional 24 hours. A luciferase assay was performed on the samples using the Dual-Luciferase Reporter Assay System (Promega). The treatment values were calculated relative to the transfection control, using the constitutively expressed Renilla construct, and the values were corrected for the positive control. N=3. Error bars depict the SEM. *p<0.05, ***P<0.001.

The genes of interest identified were: *AKR1D1*, *CYP39A1*, *CYP7B1*, *INSIG1*, *LDLR*, *LDLRAP1*, *PCSK9*, *SREBF2*, and *STARD3*. Specific primers were designed and used for qRT-PCR validation of the above genes using *HPRT1* and *SRP14* for normalization. The protein expression of the genes above was measured by Western blot and the values were calculated relative to the transfection control using the Beta tubulin loading control for normalization. The RNA and protein validation results showed minimal changes in the expression of PCSK9, SREBP2, and STARD3 (**Figure 14-16**). SiRNA-mediated knockdown of PCSK9 and STARD3 were performed as western blot negative controls to validate the specificity of the antibodies (**Supplementary Figure 4 and Supplementary Figure 6**). The SREBP-2 antibody specificity was validated using cholesterol depletion (**Supplementary Figure 5**). The RNA expression of *CYP7B1* and *LDLRAP1* remained unchanged with differential miR-1908-5p expression (**Figure 17**) but unfortunately the protein expression could not be measured due to low expression. The RNA expression of *AKR1D1* showed a decrease in expression with mimic treatment; however, the protein expression was unchanged (**Figure 18**). The RNA expression of *CYP39A1* and *INSIG1* was significantly increased by 2.4- and 1.4-fold with mimic treatment respectively (**Figure 19**). Possibly due to the low RNA expression of *CYP39A1*, the protein was undetectable by Western blot (**Supplementary Figure 7**). By comparison, the RNA expression of *INSIG1* was relatively high, however, the protein was still undetectable by Western blot (**Supplementary Figure 8**). These results suggest that *CYP7B1*, *LDLRAP1*, *PCSK9*, *SREBP2*, and *STARD3* are not target genes of miR-1908-5p.

Table 3. Lipoprotein Signaling and Cholesterol Metabolism RT2 Profiler PCR Array.

HuH-7 cells were treated with miR-1908-5p inhibitor, mimic, or transfection control using lipofectamine RNAiMAX. After 48 hours, the total RNA was isolated, cDNA was prepared and the RT2 Profiler Array (Qiagen) was performed. The expression values were normalized to the housekeeping genes: *ACTB, B2M, GAPDH, HPRT1,* and *RPLP0.* The values are relative to the transfection controls. Significance testing was performed using the FDR method. Bold represents P value < 0.05. Bold represents Q value <0.05. N=4.

	Inhibitor			**Mimic**		
Gene Name	Average	P value	Q value	Average	P value	Q value
ABCA1	1.193082	0.08106	0.4053	1.16113	0.499323	0.837978
ACAA2	0.929363	**0.000741**	**0.025935**	0.952304	0.701383	0.869627
AKR1D1	0.907122	0.17086	0.520009	0.767005	**0.046533**	0.308489
ANGPTL3	0.921202	0.245499	0.613748			
ANKRA2	0.899525	0.128268	0.483567	0.889274	0.263253	0.726578
APOA1	0.993171	0.941443	0.97073	1.081881	0.557425	0.861641
APOA2				1.282924	0.007642	0.10546
APOA4	1.001227	0.996664	0.996664	0.641346	0.005673	0.097859
APOB	0.853429	0.180216	0.52563	0.951639	0.70863	0.869627
APOC3	0.843288	0.14171	0.483567	1.105297	0.645062	0.869627
APOD	1.614317	0.110626	0.455519	0.934811	0.775996	0.895471
APOL2	0.943285	0.626692	0.827706	1.079772	0.522218	0.837978
CDH13	3.28151	**0.003452**	0.06041	0.61694	**0.02783**	0.213363
CEL	0.865039	0.13187	0.483567	1.065058	0.579095	0.861641
CETP	48.74013	0.339011	0.693119	6.548883	0.372607	0.805573
COLEC12	0.779756	**0.028351**	0.220508	0.567456	**0.000837**	0.057753
CXCL16	1.08211	0.232511	0.606369	1.19772	0.080484	0.370226
CYB5R3	1.093129	0.45219	0.718041	0.885546	0.479189	0.837978
CYP11A1	1.116814	0.366363	0.693119	1.038754	0.867953	0.909377
CYP39A1	1.063378	0.458289	0.718041	1.661028	0.026873	0.213363
CYP51A1	0.897677	**0.019744**	0.17276	1.045655	0.595093	0.861641
CYP7A1	0.809162	0.218496	0.606369			
CYP7B1	1.190238	0.626036	0.827706	6.443161	0.369179	0.805573
DHCR24	1.085887	0.399986	0.718041	1.118798	0.441943	0.837978
DHCR7	1.007188	0.956862	0.97073	0.994721	0.969751	0.974837
FDFT1	0.879479	0.088852	0.414643	1.071903	0.510016	0.837978
FDPS	0.911838	0.069239	0.389507	0.921799	0.587003	0.861641
HDLBP	1.009382	0.769534	0.913006	1.2078	0.247733	0.712232
HMGCR	0.889196	0.102802	0.449759	1.028695	0.498253	0.837978
HMGCS1	0.926817	0.445496	0.718041	1.025852	0.8238	0.902257
HMGCS2	0.925149	0.233885	0.606369	0.943809	0.785636	0.895471
IDI1	0.868615	0.064156	0.389507	1.168782	0.373834	0.805573

IDI2	1.804888	0.52763	0.785832	1.886838	0.433741	0.837978
INSIG1	0.897123	**0.007795**	0.090942	1.196223	0.171647	0.62335
INSIG2	0.875396	0.072337	0.389507	1.167802	0.369093	0.805573
LCAT	0.956945	0.612986	0.827706	1.028332	0.883018	0.909377
LDLR	0.822288	**0.000104**	**0.00728**	1.039507	0.688281	0.869627
LDLRAP1	1.218755	0.415608	0.718041	0.852197	0.361742	0.805573
LIPE	1.258258	0.355965	0.693119	0.811539	0.054039	0.308489
LRP10	1.006284	0.945814	0.97073	1.10973	0.488647	0.837978
LRP12	0.950691	0.762726	0.913006	1.029784	0.645131	0.869627
LRP1B	0.85565	0.285377	0.688841	0.850422	0.056475	0.308489
LRP6	0.957938	0.804785	0.923524	1.091665	0.599874	0.861641
LRPAP1	1.020221	0.86763	0.964033	1.284468	0.100274	0.414244
MBTPS1	0.921943	0.48454	0.737343	0.909869	0.408209	0.828424
MVD	1.037989	0.725067	0.906334	0.792935	0.235981	0.707943
MDK	0.979754	0.7583	0.913006	0.865319	0.363675	0.805573
NPC1L1	0.99189	0.916515	0.97073	1.245088	0.214785	0.673644
NROB2	0.965977	0.595988	0.827706	0.817119	0.062592	0.308489
NR1H4	1.053495	0.072133	0.389507	1.086091	0.520599	0.837978
NSDHL	1.110502	0.33917	0.693119	0.959255	0.705216	0.869627
OLR1	2.481053	0.328419	0.693119	0.414102	**0.002894**	0.066562
OSBPL1A	0.948082	0.654244	0.832674	0.972666	0.804626	0.895471
PCSK9	0.980105	0.788766	0.920227	0.763048	0.10206	0.414244
PMVK	1.007871	0.927782	0.97073	0.96447	0.729849	0.869627
PPARD	1.047747	0.85637	0.964033	0.80278	**0.013007**	0.149581
PRKAA1	0.917177	0.418677	0.718041	1.147469	0.190885	0.643474
PRKAA2	0.883398	0.169013	0.520009	1.516652	0.109146	0.418393
PRKAG2	0.849921	**0.005914**	0.082796	0.865508	0.354476	0.805573
SCAP	0.929365	0.352948	0.693119	0.993274	0.974837	0.974837
SCARF1	1.680311	0.342214	0.693119	1.069239	0.866778	0.909377
SNX17	1.089691	0.461598	0.718041	0.975102	0.700232	0.869627
SOAT1	0.977835	0.884663	0.9676	1.023215	0.7989	0.895471
SORL1	0.750429	**0.002599**	0.06041	1.03969	0.730991	0.869627
SREBF1	1.085177	0.651832	0.832674	0.731582	**0.00263**	0.066562
SREBF2	1.053181	0.446065	0.718041	1.022999	0.87756	0.909377
STAB2	49.9238	0.359014	0.693119	0.822871	0.61189	0.861641
STARD3	1.342056	**0.01947**	0.17276	0.845941	0.061006	0.308489
TM7SF2	1.056564	0.596643	0.827706	0.856268	0.19584	0.643474
TRERF1	1.13079	0.619042	0.827706	3.089581	0.385274	0.805573
VLDLR	0.833984	0.14507	0.483567	0.808102	**0.023738**	0.213363

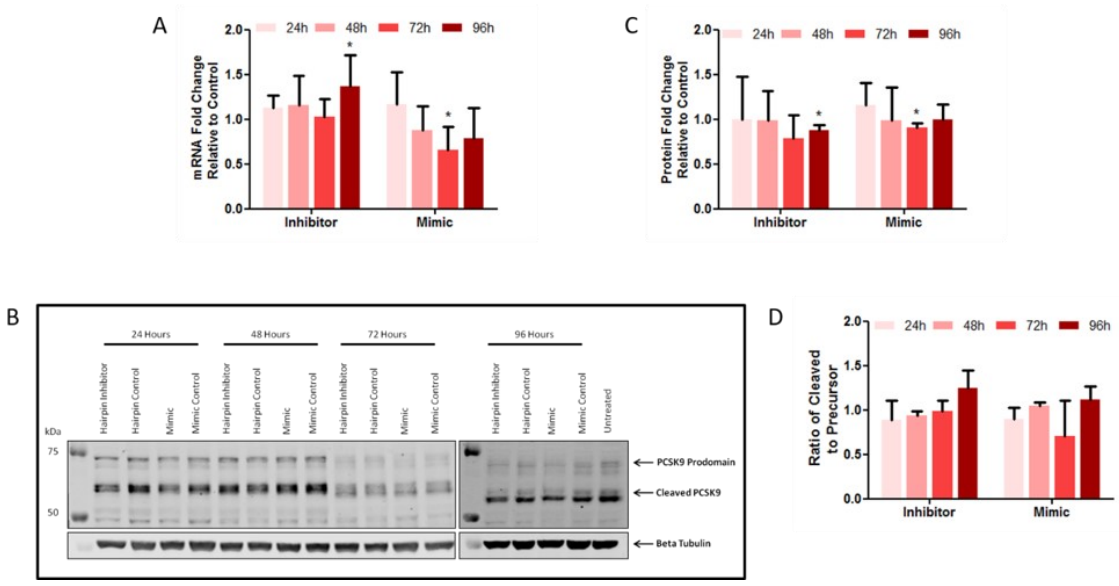

Figure 14. PCSK9 expression remains unchanged with differential miR-1908-5p expression.

HuH-7 cells were treated with 9 nM of miR-1908-5p inhibitor, mimic, or transfection control. (A) *PCSK9* mRNA expression was analyzed using qRT-PCR. The mean fold change was calculated relative to the transfection control using *HPRT1 and SRP14* for normalization for 5 independent experiments. (B) A Western blot was performed using Beta tubulin as a loading control to measure (C) the mean fold change in total PCSK9 protein expression and (D) the ratio of cleaved PCSK9 to the prodomain relative to the transfection control for 3 independent experiments. Error bars depict the SD. *$p<0.05$.

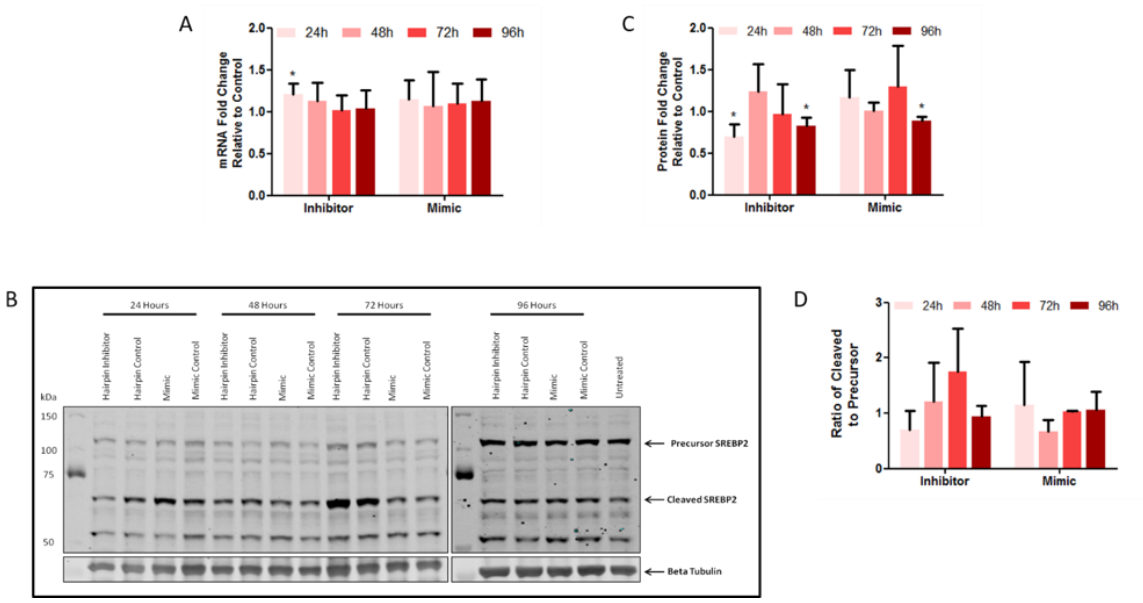

Figure 15. SREBP2 expression remains unchanged with differential miR-1908-5p expression.

HuH-7 cells were treated with 9 nM of miR-1908-5p inhibitor, mimic, or transfection control. (A) *SREBP2* mRNA expression was analyzed using qRT-PCR. The mean fold change was calculated relative to the transfection control using *HPRT1 and SRP14* for normalization for 5 independent experiments. (B) A Western blot was performed using Beta tubulin as a loading control to measure (C) the mean fold change in total SREBP2 protein expression and (D) the mean ratio of cleaved to precursor SREBP2 relative to the transfection control for 3 independent experiments. Error bars depict the SD. *p<0.05.

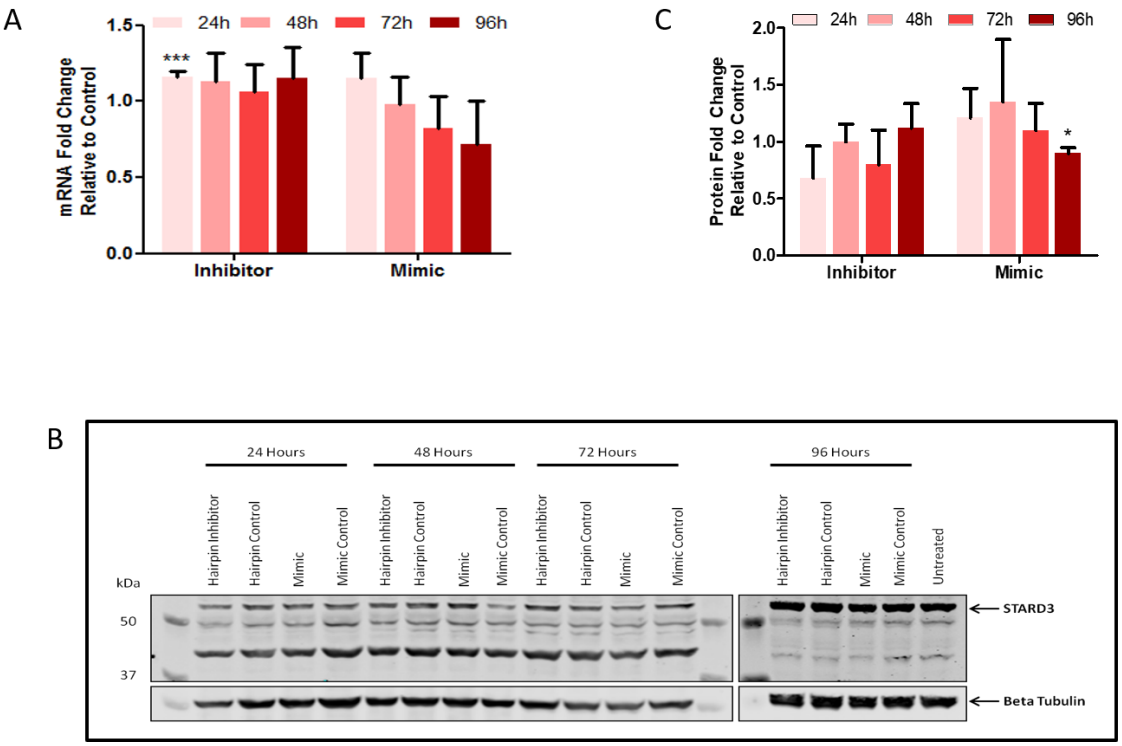

Figure 16. STARD3 expression remains unchanged with differential miR-1908-5p expression.

HuH-7 cells were treated with 9 nM of miR-1908-5p inhibitor, mimic, or transfection control. (A) *STARD3* mRNA expression was analyzed using qRT-PCR. The mean fold change was calculated relative to the transfection control using *HPRT1 and SRP14* for normalization for 5 independent experiments. (B) A Western blot was performed using Beta tubulin as a loading control to measure (C) the mean fold change in STARD3 protein expression relative to the transfection control for 3 independent experiments. Error bars depict the SD. *p<0.05, ***p<0.001.

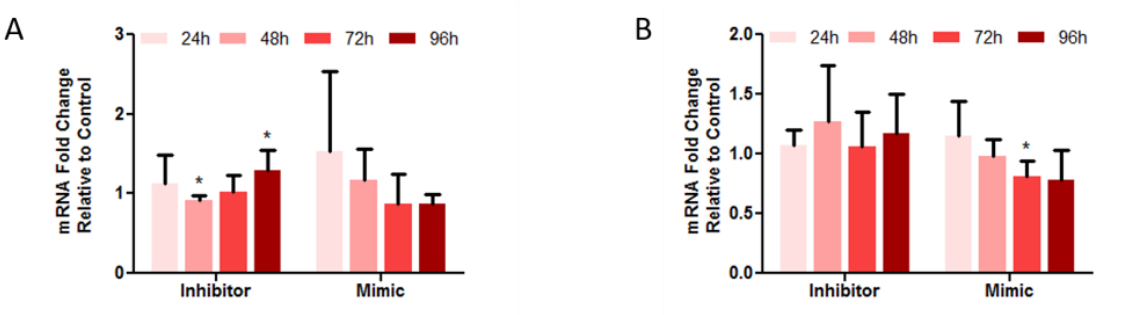

Figure 17. The RNA expression of *CYP7B1* and *LDLRAP1* remains unchanged with differential miR-1908-5p expression.
HuH-7 cells were treated with 9 nM of miR-1908-5p inhibitor, mimic, or transfection control. (A) *CYP7B1* and (B) *LDLRAP1* expression was analyzed using qRT-PCR. The fold change was calculated as treatment relative to transfection control and HPRT1 and SRP14 were used for normalization. N=5. Error bars depict SD. *p<0.05.

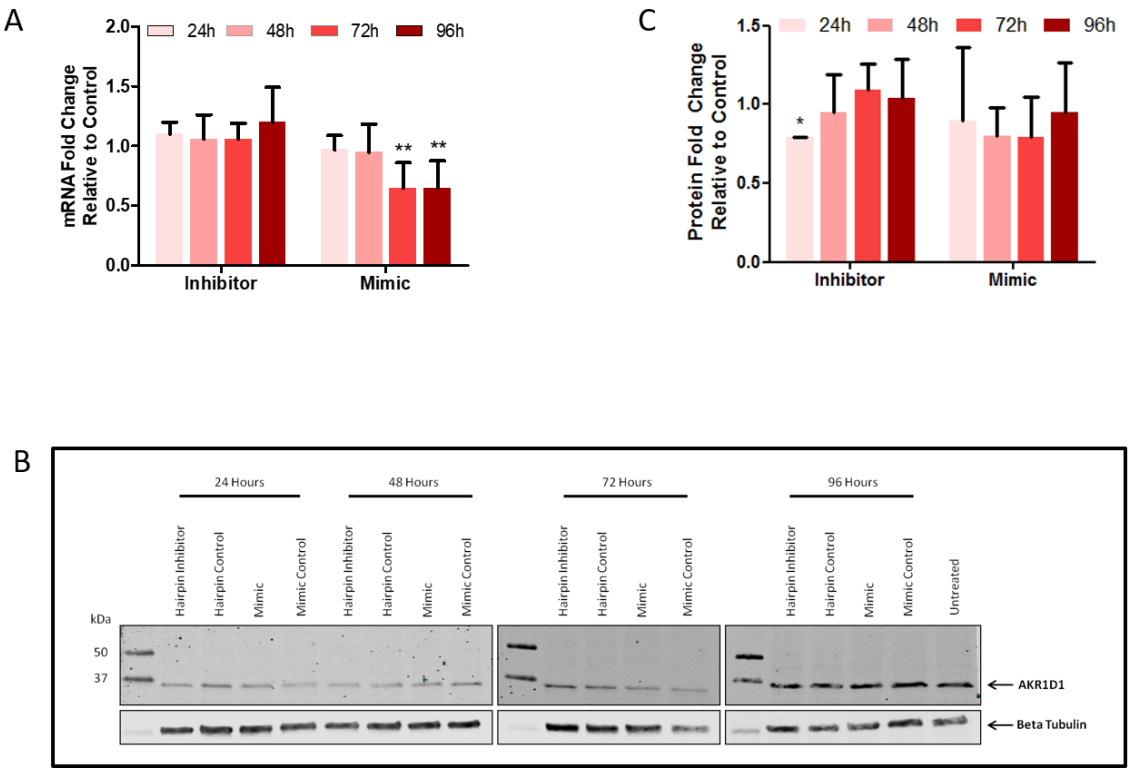

Figure 18. AKR1D1 expression remains unchanged with differential miR-1908-5p expression.

HuH-7 cells were treated with 9 nM of miR-1908-5p inhibitor, mimic, or transfection control. (A) *AKR1D1* mRNA expression was analyzed using qRT-PCR. The mean fold change was calculated relative to the transfection control using *HPRT1 and SRP14* for normalization for 5 independent experiments. (B) A Western blot was performed using Beta tubulin as a loading control to measure (C) the mean fold change in AKR1D1 protein expression relative to the transfection control for 3 independent experiments. Error bars depict the SD. *p<0.05.

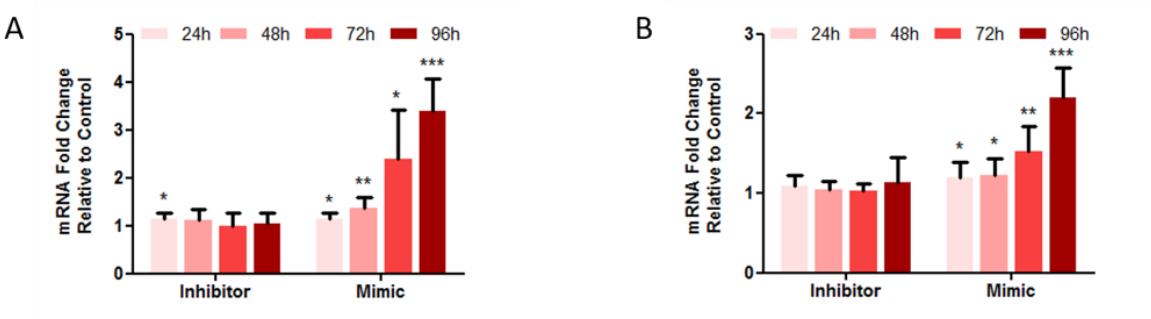

Figure 19. Increased RNA expression of *CYP39A1* and *INSIG1* with miR-1908-5p mimic treatment.

HuH-7 cells were treated with 9 nM of miR-1908-5p inhibitor, mimic, or transfection control. (A) *CYP39A1* and (B) *INSIG1* expression was analyzed using qRT-PCR. The fold change was calculated as treatment relative to transfection control and HPRT1 and SRP14 were used for normalization. N=5. Error bars depict SD. *p<0.05, **p<0.01, ***p<0.001.

As for CYP39A1 and INSIG1, our preliminary data suggests a potential indirect relationship with miR-1908-5p but further studies are needed to validate these changes at the protein level. Based on the CYP39A1 findings, the bile acid metabolism pathway was further studied by validating CYP27A1. The RNA and protein expression were measured and calculated as described above. Although the RNA expression of CYP27A1 showed a significant decrease with mimic treatment, the protein expression remained unchanged (**Figure 20**). SiRNA-mediated knockdown of CYP27A1 was performed as a western blot negative control to validate antibody specificity (**Supplementary Figure 9**).

Interestingly, the RNA expression and total protein expression of LDLR remained unchanged with inhibitor and mimic treatment, however the ratio of the mature (160 kDa) to the cleaved (125 kDa) band of LDLR was significantly increased after 96 hours of mimic treatment and there was a trend towards a decrease after 96 hours of inhibitor treatment (**Figure 21**). This intriguing finding suggests a relationship between hepatocyte expression of miR-1908-5p and cleavage of LDLR, that may be relevant to the association of miR-1908-5p to plasma concentrations of LDL-cholesterol.

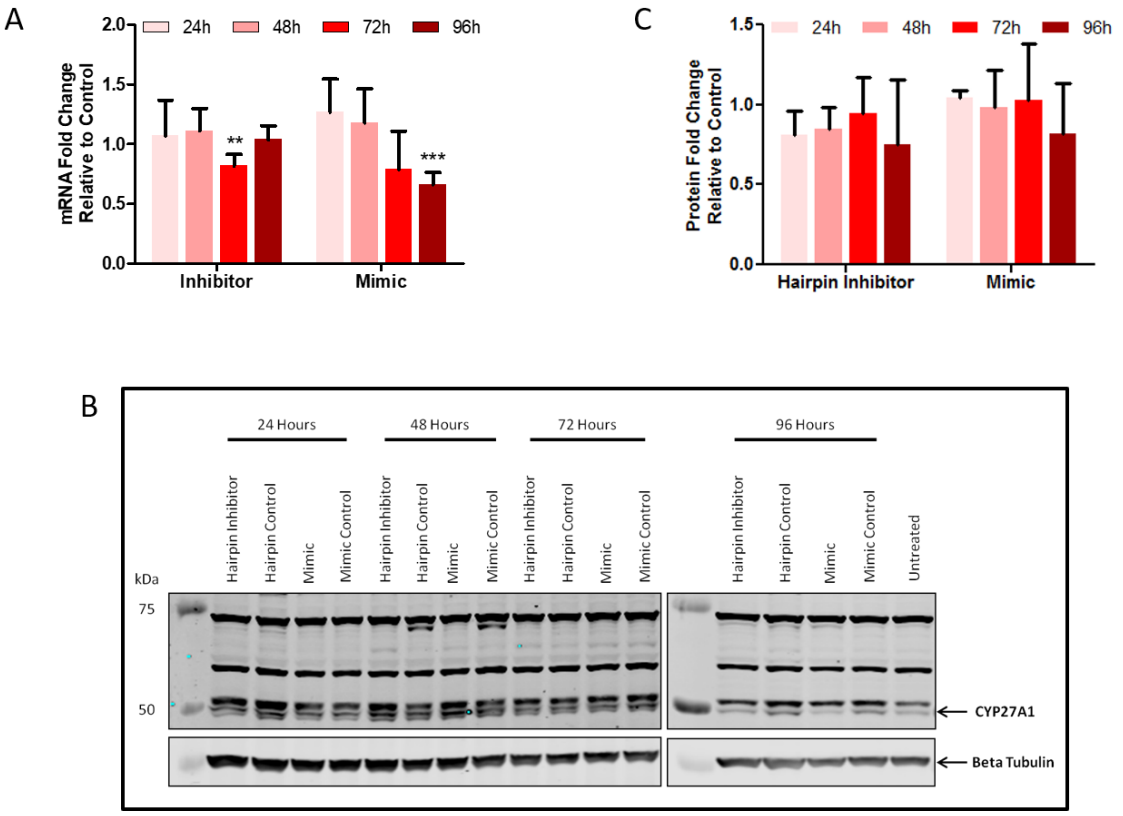

Figure 20. CYP27A1 expression remains unchanged with differential miR-1908-5p expression.

HuH-7 cells were treated with 9 nM of miR-1908-5p inhibitor, mimic, or transfection control. (A) *CYP27A1* mRNA expression was analyzed using qRT-PCR. The mean fold change was calculated relative to the transfection control using *HPRT1 and SRP14* for normalization for 5 independent experiments. (B) A Western blot was performed using Beta tubulin as a loading control to measure (C) the mean fold change in CYP27A1 protein expression relative to the transfection control for 3 independent experiments. Error bars depict the SD. **p<0.01, ***p<0.001.

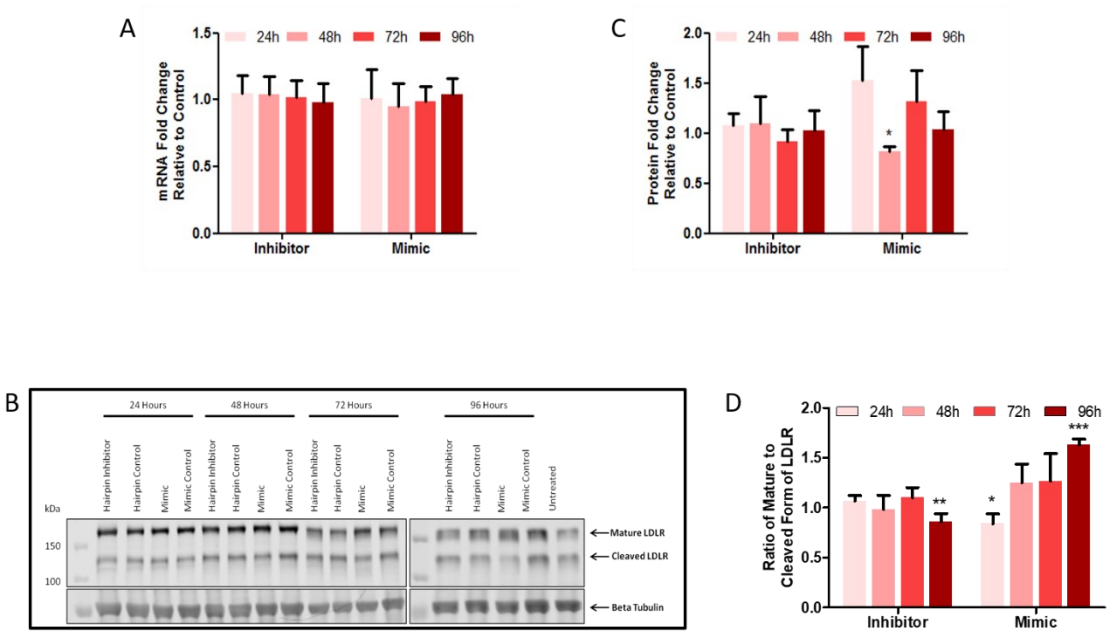

Figure 21. Increased ratio of mature to cleaved LDLR with 96h miR-1908-5p mimic treatment.

HuH-7 cells were treated with 9 nM of miR-1908-5p inhibitor, mimic, or transfection control. (A) *LDLR* mRNA expression was analyzed using qRT-PCR. The mean fold change was calculated relative to the transfection control using HPRT1 and SRP14 for normalization for 5 independent experiments. (B) A Western blot was performed using Beta tubulin as a loading control to measure (C) the mean fold change in total LDLR protein expression and (D) the mean ratio of mature to cleaved LDLR relative to the transfection control for 5 independent experiments for the inhibitor treatment and 3 independent experiments for the mimic treatment. Error bars depict the SD. *p<0.05, ***p<0.001.

4. Discussion

Leveraging miRNA-Seq data and 1000 Genomes imputed genotypes, our laboratory identified rs174561-C, previously associated with plasma levels of LDL-C, as a strong miRQTL for miRNA-1908-5p measured by RNASeq ($P=4.8x10^{-31}$) [31]. We further demonstrated an inverse relationship between circulating miR-1908-5p and circulating LDL-C, fasting glucose and A1c [31]. Here I have investigated the molecular mechanism (s) linking miR-1908-5p to cholesterol metabolism.

Ghanbari *et al*. reported that presence of the C allele for rs174561 is thermodynamically more stable for the predicted secondary structure of pre-miR-1908 than the T allele [42]. Our results show that overexpression of the minor C allele for rs174561 in HuH-7 cells leads to higher expression of miR-1908-5p compared to the T allele (**Figure 6)**. Future experiments could determine if this effect is due to increased stability of the miR-1908-5p strand or increased degradation of the miR-1908-3p strand. This association is difficult to study *in vivo* because the expression of miR-1908-5p is limited to humans and other primates [31]. The minor allele frequency (MAF) of rs174561 is 0.30 in a European population. In further studies, the association of this SNP with expression of miR-1908-5p can be confirmed using human liver biopsies or in adipose tissue biopsies since Guang-feng *et al.* demonstrated that miR-1908 is involved in adipocyte differentiation and metabolism [40]. It will also be of interest to investigate the tissue specific functions of circulating miR-1908 since miRNAs can be secreted into extracellular fluids for delivery to various tissue, where they function as intercellular signaling molecules due to their autocrine, endocrine, or paracrine modes of regulation [33].

Our previous studies indicated a potential role of miR-1908 in cholesterol metabolism [31]. Cholesterol homeostasis is a tightly regulated process in hepatocytes where changes in the expression of key regulatory genes alter cholesterol uptake or secretion [5]. My findings demonstrate for the first time that cholesterol depletion in HuH-7 cells leads to increased expression of miR-1908-5p, while cholesterol loading has the opposite effect (**Figure 7 and 8**). Of note, the expression of miR-1908-5p is higher than the expression of miR-1908-3p in HuH-7 cells which may confer greater functionality of miR-1908-5p in these cells (data not shown). The effects of altering cellular cholesterol were not as robust for miR-1908-3p, which could be explained by its lower expression relative to miR-1908-5p (**Figure 7 and 8**). These findings support a role for miR-1908-5p in hepatocellular response to altered cholesterol availability and await confirmation in HepaRG cells or primary hepatocytes. HuH-7 cells are hepatocyte-derived carcinoma cells and like many other cancer cells, they are genetically unstable and they can undergo rearrangements depending on cell line maintenance and passage number [43]. As shown in **Supplementary Figure 1**, when the exogenous cholesterol supply was minimized, it did not result in a significant decrease in total cellular cholesterol. Furthermore, the supply of exogenous cholesterol provided by 10% FBS media conditions did not allow for the maintenance of cholesterol homeostasis with rosuvastatin treatment. These findings suggest that HuH-7 cells are more reliant on cholesterol synthesis as compared to *in vivo* hepatocytes. This observation is in agreement with published data but it is surprising nonetheless because in humans, the liver accounts for only 10% of total cholesterol synthesis and 70% of LDL clearance [44]. Although the results found in HuH-7 cells cannot be assumed to be entirely comparable to *in vivo* hepatocyte

conditions, with the proper cell maintenance, use of appropriate controls, and validation in other models, HuH-7 cells are a valuable starting point for *in vitro* hepatocyte research [45].

Next, the HuH-7 cells were treated with a miR-1908-5p inhibitor or mimic to determine if differential miR-1908-5p expression affects the level of total cholesterol, free cholesterol, or cholesteryl esters. While inhibitor and mimic treatment both resulted in a trend towards an increase in free cholesterol, the level of total cholesterol remained unchanged (**Figure 9**). The cholesteryl esters were calculated as the difference between the total and free cholesterol. A 20% decrease in cholesteryl esters was observed with mimic treatment; however, the opposite effect was not observed with the inhibitor treatment. This was not surprising because the effect of miRNAs on its target genes are relatively mild and the effect may not be observable due to the tight regulation of cholesterol homeostasis within the cells [46]. Very few miRNA deletions result in lethal phenotypes or major abnormalities, therefore differential miR-1908-5p expression was not expected to result in drastic changes in cellular cholesterol as this would be lethal to the cells [46]. To validate the effect of differential miR-1908-5p expression on cholesteryl esters and to determine a potential cellular mechanism, the activity of ACAT1 and ACAT2 encoded by *SOAT1* and *SOAT2* respectively is of interest. These enzymes are responsible for cholesterol esterification that serves to protect the cell from the toxic effects of over accumulation of free cholesterol in cell membranes [47]. These experiments may reveal a potential role of miR-1908-5p in decreasing hepatic cholesteryl esters which

could promote LDL-cholesterol uptake from circulation to maintain cholesterol homeostasis.

After demonstrating the dependence of miR-1908-5p expression on cellular cholesterol, a mechanistic approach was taken to determine target genes of miR-1908-5p related to cholesterol metabolism. Most functional studies of miR-1908-5p have been focused on the field of cancer. One study in metastatic cells identified *APOE* as a target gene of miR-1908, miR-199a-3p, and miR-199a-5p which act in a synergistic manner [37]. *APOE* is the major ligand responsible for the binding of chylomicron remnants, HDL, and VLDL particles to various hepatic receptors allowing for their clearance from circulation [10]. To determine if miR-1908-5p can independently target *APOE* in a liver model, HuH-7 cells were treated with a miR-1908-5p inhibitor or mimic. A slight inverse effect was observed on the RNA expression of *APOE*; however, the effect was diminished at the protein level (**Figure 10**). Our results suggest that *APOE* is not a major target of miR-1908-5p alone in the liver. To further investigate the convergent effect of miR1908, miR-199a-3p, and miR-199a-5p in a hepatoma cell model, these miRNAs could be treated individually with an inhibitor or a mimic or they could be convergently targeted. This would determine if the inverse effect on *APOE* is associated with the activity of all 3 miRNAs, similar to cancer metastasis, or if one of them can exert this effect individually. Two other genes important for chylomicron and VLDL metabolism are *FADS1* and *FADS2*. When chylomicron remnants are cleared by the liver, the dietary fatty acids are processed by FADS1 and FADS2 into phospholipids, triacylglycerols, and cholesteryl esters which are required for the formation of VLDL

particles [21]. As previously mentioned, rs174561 is a miRQTL for miR-1908-5p (P_{miRQTL}= 4.8E-31), but it has also been identified as an eQTL for *FADS1* in the liver (P_{eQTL}= 1.8E-6) [31,48]. While rs174561 is not an eQTL for *FADS2* in the liver, in the GTExPortal there is a strong association in many other tissues including subcutaneous adipose tissue (P_{eQTL}= 4.0E-7) [48]. The genomic location of this SNP overlaps with the location of miR-1908 in the first intron of *FADS1* which is slightly downstream of *FADS2* [49]. Although functional links between miRNAs and their host genes are rare, a potential relationship still exists [50]. Due to the association of *FADS1* and *FADS2* with our SNP of interest, their close genomic proximity to miR-1908-5p, and their role in lipoprotein metabolism, these genes were tested as potential target genes of miR-1908-5p. Following inhibitor and mimic treatment, there was no observable effect on *FADS1* or *FADS2* expression, therefore we can conclude that rs174561 has pleiotropic and independent effects (**Figure 11 and 12**).

To identify potential signaling pathways that are affected by differential miR-1908-5p expression, a Cignal 45-Pathway Reporter Array was performed in HuH-7 cells. With inhibitor treatment, an increase in *HIF1A* encoding the HIF-1α transcription factor which regulates the hypoxia signaling pathway was observed; however, the mimic treatment also showed a trend towards an increase (**Figure 13**). When the expression of HIF-1α is stimulated, the hypoxia signaling pathway regulates extracellular matrix remodeling, energy metabolism, autophagy and cell motility [51]. Induction of the hypoxia pathway typically results in reduced cell proliferation to regulate the oxygen demand. However, many cancer cell populations, can maintain cell proliferation under hypoxic conditions [51]. These

findings could further support a role for miR-1908-5p in promoting cell proliferation and survival in a cancer model as reported in the literature but the lack of opposite effects of mimic and inhibitor on *HIF1A* expression requires further explanation. We also observed a significant decrease in *TGFB1* encoding TGF-β with mimic treatment, while the inhibitor treatment showed no change (**Figure 13**). TGF-β1 promotes cell proliferation and it can also regulate cell growth and differentiation [52]. Previous studies have shown that miR-1908 inhibits the expression of TGF-β1 in the myocardial infarction border zone, thereby improving cardiac fibrosis after myocardial infarction by reducing cell proliferation [52]. Taken together, these results support a role of miR-1908 in regulating proliferation; however, the directionality remains unclear and requires further investigation. Future experiments could test the dependence of miR-1908 expression on these pathways by treating HuH-7 cells with drugs that inhibit the hypoxia and TGF-β1 signalling pathways.

The final goal of my project was to determine targets of miR-1908-5p related to cholesterol metabolism. A PCR array was used to look for changes in genes related to lipoprotein signaling and cholesterol metabolism as a result of differential miR-1908-5p expression (**Table 3**). A false discovery rate was calculated to determine significant changes in gene expression; however, only 2 genes, *ACAA2* and *LDLR*, were identified. I chose not to follow up on *ACAA2* because of the small effect size. Due to the stringency of FDR testing, I used a combination of the nominal P values and directional consistencies between the inhibitor and mimic treatments to identify 5 genes of interest: *AKR1D1*, *CYP39A1*, *CYP7B1*, *INSIG1*, and *STARD3*. In parallel with the validation of *LDLR*, I also chose to follow up on

LDLRAP1, *PCSK9*, and *SREBF2* because they were identified as predicted targets of miR-1908-5p by TargetScan and they are closely associated with the expression and stability of LDLR [53]. It is important to err on the side of caution with computer-predicted miRNA targets because they are based on sequence specificity therefore there may be both false positives and missed functional miRNA targets [54].

When intracellular cholesterol levels rise above the normal threshold, the major pathway responsible for sustaining cholesterol homeostasis is bile acid synthesis [25]. There are 3 different sterol 7α-hydroxylases that are involved in the conversion of cholesterol into bile acids. The first enzyme responsible for converting cholesterol into 7α-hydroxycholesterol is CYP7A1 [25]. Although the array results showed very low expression of *CYP7A1*, the downstream *AKR1D1* enzyme was better expressed and identified as a gene of interest. The RNA and protein expression of AKR1D1 remained unchanged with inhibitor treatment (**Figure 18**). Treatment with miR-1908-5p mimic resulted in a significant decrease in *AKR1D1* RNA expression but a diminished effect was observed for protein expression (**Figure 18**). The low expression of the rate limiting enzyme, *CYP7A1*, and the small effect size of differential miR-1908-5p expression on AKR1D1 protein expression suggests that the classic bile acid synthesis pathway is not affected by miR-1908-5p in HuH-7 cells. CYP7B1 is the alternative pathway enzyme responsible for preferentially converting 25-, and 27-hydroxycholesterol into 5-cholesten-3α,7α-triols [26]. The RNA expression of *CYP7B1* increased slightly with inhibitor treatment with a trend towards a decrease with mimic treatment (**Figure 17**). More interestingly, the RNA expression of *CYP39A1* remained unchanged with inhibitor treatment;

however, a significant 3-fold increase was observed with mimic treatment (**Figure 19**). CYP39A1 is the alternative pathway enzyme that preferentially converts 24-hydroxycholesterol from the brain into 5-cholesten-3α,7α,24(S)-triol [26]. To extend these findings, I measured the expression of CYP27A1 which is the next enzyme involved in the bile acid synthesis pathway and found no change in its protein expression with differential miR-1908-5p expression (**Figure 20**). These results do not accord with the *CYP39A1* findings because it is predicted that the levels of CYP27A1 would increase as a result of higher substrate synthesis. Although the mechanism is unclear, these findings are intriguing because they suggest a potential role for miR-1908 in regulating the conversion of 24-hydroxycholesterol which is derived from cholesterol in the brain and transported to the liver [26]. Future studies in bile acid metabolomics are needed to determine which bile acid intermediates or final products are affected by differential miR-1908-5p expression.

When intracellular cholesterol levels fall below a certain threshold, SCAP is no longer bound to cholesterol allowing for dissociation of INSIG1 from the SCAP/SREBP2 complex [5]. This results in transportation of the complex to the Golgi apparatus where SREBP2 is further processed into its active transcription factor which can bind to the SRE in the promoter of downstream target genes involved in cholesterol uptake and synthesis, thereby inducing transcription [5]. *HMGCR* is one of the genes affected by SREBP2 and it is responsible for intracellular cholesterol synthesis in the ER [5]. Once synthesized, this cholesterol can be transported from the ER to the cellular membrane or endosomal membrane by STARD3 or it can be esterified and stored in the form of lipid droplets [23,24]. Two other genes under the

control of SREBP2 that are involved in the cholesterol uptake pathway are *PCSK9* and *LDLR* [5]. Following miR-1908-5p mimic treatment, the RNA expression of *INSIG1* was significantly increased by 2-fold, while inhibitor treatment failed to display an opposite effect (**Figure 19**). These results could not be confirmed at the protein level because despite multiple attempts, INSIG1 was undetectable by western blot. This could be due to the difficulty of isolating INSIG1 since it is embedded in the ER membrane. Microscopy studies may be required to evaluate if there are any INSIG1 protein changes. Although the expression of *INSIG1* was increased with mimic treatment, the RNA and protein expression of SREBP2 remained unchanged with both inhibitor and mimic treatment (**Figure 15**). The ratio of the cleaved form to the precursor of SREBP2 also remained unchanged with both treatments (**Figure 15**).

Taken together, these observations allude to a potential role of miR-1908 in regulating lipogenesis through increased expression of *INSIG1*. Since the active form of SREBP2 remained unchanged, we expected the RNA and total protein expression of its downstream target genes to also remain unchanged. HMGCR was measured on the qPCR array but its expression did not dramatically change with the inhibitor or mimic treatment; therefore, we chose not to validate its expression. There was also no change observed for the protein expression of STARD3 with differential miR-1908-5p expression which was not surprising because we did not see an increase in the synthesis of intracellular cholesterol (**Figure 16**).

PCSK9 is also under the transcriptional control of SREBP2. Its RNA expression was slightly decreased with mimic treatment; however, the total protein

expression and the ratio of cleaved to precursor PCSK9 remained unchanged (**Figure 14**). The SREBP2 and PCSK9 findings suggest that the RNA and total protein expression of LDLR should remain unchanged with differential miR-1908-5p expression. This hypothesis was proven to be true for the RNA expression of *LDLR* but of note, there was a slight trend towards an increase with mimic treatment for the total LDLR protein expression (**Figure 21**). More interestingly, we observed an increase in the ratio of the mature to the cleaved form of LDLR after 96 hours of mimic treatment (**Figure 21**). The 96-hour inhibitor treatment resulted in a trend towards a decrease which in further studies we could potentially augment by cholesterol depleting the HuH-7 cells to increase the background expression of LDLR before treating the cells with the miR-1908-5p inhibitor.

Importantly, these findings indicate that although the miR-1908-5p mimic does not affect the total expression of LDLR, it reduces the cleavage of the mature LDLR. The proteolytic fragment of LDLR was first discovered by Lehrman *et al* in 1985 [55]. More recently, it has been reported that bone morphogenetic protein-1 (BMP1) is responsible for the proteolytic cleavage of LDLR in its extracellular ligand-binding domain and that the resulting 125 kDa fragment has a reduced capacity for LDL binding and uptake in HepG2 cells [56,57]. Future studies are planned to confirm the effect of differential miR-1908-5p expression on reducing the cleavage of LDLR by performing pulse chase experiments with radiolabelled methionine to track to the rate of cleavage over time. It will also be important to determine if this effect is occurring through the targeting of BMP1 by miR-1908-5p or if miR-1908-5p targets other LDLR cleavage proteins. In ongoing studies in our laboratory, we are

attempting to determine direct mRNA binding partners of miR-1908-5p by Argonaut (AGO2) pulldown on cells treated with miR-1908 inhibitor or mimic followed by RNA sequencing. Although further investigation is needed to confirm the direct mechanism of miR-1908-5p in reducing LDLR cleavage, these studies suggest a potential model whereby increased miR-1908-5p expression reduces LDLR cleavage allowing for increased uptake of LDL-cholesterol from circulation.

Central to the above findings, it is important to note that in general, the effects of miRNAs on their target gene expression is relatively small which supports a role for fine-tuning rather than a major regulatory role [33]. It is also necessary to consider the off-target effects of miRNA mimics, especially when the directionality is inconsistent with the inhibitor treatment. Off-target effects of miRNA mimics can be caused by the seed sequence of the miRNA and they often depend on the ability of the sense or antisense strand to be assembled onto the RISC [33]. The miRNA mimics used in this thesis are double stranded RNA oligonucleotides that have chemical enhancements on the guide strand to preferentially bind to the RISC, thereby reducing the number of off-target effects [58]. Off-target effects can also result from binding of miRNAs to mRNAs with only partial complementarity and these off-target effects are often enhanced with mimic treatment due to the high levels of overexpression compared with the endogenous levels [33]. Very few papers to date have reported off-target effects caused by miRNAs but many reports have discussed issues of overexpressing miRNAs due to their multi-targeting of various mRNAs which can lead to off-target toxicity [59]. For example, here I have demonstrated the potential of miR-1908-5p to regulate LDLR cleavage, but it has also been shown to

regulate cell proliferation. Due to the issues of tissue specific delivery of miRNAs, major off-target effects result from systemic overexpression of miRNAs [59]. One way to overcome this is to use multiple miRNAs that have the same target gene so that the doses of the individual miRNAs are reduced in an attempt to reduce the off-target effects [60]. With future studies in the field of miRNA-based therapeutics and advancements in tissue specific delivery, there may be a benefit to using these therapies in combination with statins or bile acid sequestrants to reduce the levels of circulating LDL-cholesterol.

5. Conclusion

Here, I have explored at a molecular and cellular level, the biology underlying the novel finding from our laboratory that rs174561, a SNP intronic to *FADS1*, is a miRQTL for miR-1908-5p, that in turn associates with plasma LDL-C [31]. I have provided evidence that the presence of the C vs T allele of rs174561 leads to higher expression of miR-1908-5p in HuH-7 cells. I have also demonstrated the association of miR-1908-5p expression with cellular cholesterol levels.

A lipoprotein signaling and cholesterol metabolism qPCR array was then used to identify target genes affected by differential miR-1908-5p expression. RNA and protein validation experiments revealed *CYP39A1, INSIG1,* and *LDLR* as genes of interest and I chose to follow up on the latter due to its central importance in the regulation of plasma LDL-C concentrations. Validation experiments demonstrated no change in total RNA or protein expression of LDLR with differential miR-1908-5p expression. Importantly; however, the ratio of the mature 160kDa band to the cleaved 125kDa band was decreased by 0.85-fold with inhibitor treatment and was increased by 1.63-fold following mimic treatment. Consistent with an association of miR-1908-5p with LDL-C, cleavage of the mature LDLR results in reduced binding and cellular uptake of LDL [56].

Future experiments are required to identify the direct target gene of miR-1908-5p mediating LDLR cleavage. Pulse chase experiments may be used to detect differences in the rate of cleavage between the mimic and control treatments. In summary, the experiments described in this thesis elucidate a potential mechanism

linking miR-1908-5p to lower circulating LDL-cholesterol levels through reduced cleavage of the mature LDLR.

6. References

1. Cardiovascular diseases (CVDs). https://www.who.int/en/news-room/fact-sheets/detail/cardiovascular-diseases-(cvds). Accessed November 18, 2019.
2. Lusis AJ. Atherosclerosis. doi:10.1038/35025203
3. Williams KJ, Tabas I. The response-to-retention hypothesis of early atherogenesis. *Arterioscler Thromb Vasc Biol*. 1995;15(5):551-562. doi:10.1161/01.atv.15.5.551
4. Nakashima Y, Fujii H, Sumiyoshi S, Wight TN, Sueishi K. Early human atherosclerosis: Accumulation of lipid and proteoglycans in intimal thickenings followed by macrophage infiltration. *Arterioscler Thromb Vasc Biol*. 2007;27(5):1159-1165. doi:10.1161/ATVBAHA.106.134080
5. Goldstein JL, Brown MS. Leading Edge Review A Century of Cholesterol and Coronaries: From Plaques to Genes to Statins. *Cell*. 2015;161:161-172. doi:10.1016/j.cell.2015.01.036
6. Tabas I, García-Cardeña G, Owens GK. Recent insights into the cellular biology of atherosclerosis. *J Cell Biol*. 2015;209(1):13-22. doi:10.1083/jcb.201412052
7. Glass CK, Witztum JL. Atherosclerosis: The road ahead. *Cell*. 2001;104(4):503-516. doi:10.1016/S0092-8674(01)00238-0
8. Tabas I, Williams KJ, Borén J. Subendothelial lipoprotein retention as the initiating process in atherosclerosis: Update and therapeutic implications. *Circulation*. 2007;116(16):1832-1844. doi:10.1161/CIRCULATIONAHA.106.676890
9. Mundi S, Massaro M, Scoditti E, et al. Endothelial permeability, LDL deposition, and cardiovascular risk factors-A review. *Cardiovasc Res*. 2018;114(1):35-52. doi:10.1093/cvr/cvx226
10. Feingold KR, Grunfeld C. *Introduction to Lipids and Lipoproteins*.; 2000. http://www.ncbi.nlm.nih.gov/pubmed/26247089. Accessed November 21, 2019.
11. Charlton-Menys V, Durrington PN. Human cholesterol metabolism and therapeutic molecules. *Exp Physiol*. 2007;93:27-42. doi:10.1113/expphysiol.2006.035147
12. Goedeke L, Fernández-Hernando C. Regulation of cholesterol homeostasis. *Cell Mol Life Sci*. 2012;69(6):915-930. doi:10.1007/s00018-011-0857-5
13. Ponziani FR, Pecere S, Gasbarrini A, Ojetti V. Physiology and pathophysiology of liver lipid metabolism. *Expert Rev Gastroenterol Hepatol*. 2015;9(8):1055-1067. doi:10.1586/17474124.2015.1056156
14. Lu K, Lee MH, Patel SB. Dietary cholesterol absorption; more than just bile. *Trends Endocrinol Metab*. 2001;12(7):314-320. doi:10.1016/S1043-2760(01)00433-7
15. Kawano Y, Cohen DE. Mechanisms of hepatic triglyceride accumulation in non-alcoholic fatty liver disease. *J Gastroenterol*. 2013;48(4):434-441. doi:10.1007/s00535-013-0758-5
16. Berberich AJ, Hegele RA. The complex molecular genetics of familial hypercholesterolaemia. *Nat Rev Cardiol*. 2019;16(1):9-20.

doi:10.1038/s41569-018-0052-6
17. Lange Y, Ye J, Chin J. The fate of cholesterol exiting lysosomes. *J Biol Chem*. 1997;272(27):17018-17022. doi:10.1074/jbc.272.27.17018
18. Lagace TA. PCSK9 and LDLR degradation: Regulatory mechanisms in circulation and in cells. *Curr Opin Lipidol*. 2014;25(5):387-393. doi:10.1097/MOL.0000000000000114
19. SREBPs: activators of the complete program of cholesterol and fatty acid synthesis in the liver. https://www.ncbi.nlm.nih.gov/pmc/articles/PMC150968/. Accessed November 26, 2019.
20. Eberlé D, Hegarty B, Bossard P, Ferré P, Foufelle F. SREBP transcription factors: Master regulators of lipid homeostasis. *Biochimie*. 2004;86(11):839-848. doi:10.1016/j.biochi.2004.09.018
21. Liu JJ, Green P, Mann JJ, Rapoport SI, Sublette ME. Pathways of Polyunsaturated Fatty Acid Utilization: Implications for Brain Function in Neuropsychiatric Health and Disease NIH Public Access. 2016. doi:10.1016/j.brainres.2014.11.059
22. Sundqvist A, Bengoechea-Alonso MT, Ye X, et al. Control of lipid metabolism by phosphorylation-dependent degradation of the SREBP family of transcription factors by SCFFbw7. *Cell Metab*. 2005;1(6):379-391. doi:10.1016/j.cmet.2005.04.010
23. Wilhelm LP, Wendling C, Védie B, et al. <scp>STARD</scp> 3 mediates endoplasmic reticulum-to-endosome cholesterol transport at membrane contact sites. *EMBO J*. 2017;36(10):1412-1433. doi:10.15252/embj.201695917
24. Gulati S, Balderes D, Kim C, et al. ATP-binding cassette transporters and sterol O-acyltransferases interact at membrane microdomains to modulate sterol uptake and esterification. *FASEB J*. 2015;29(11):4682-4694. doi:10.1096/fj.14-264796
25. Russell DW. Fifty years of advances in bile acid synthesis and metabolism. 2009. doi:10.1194/jlr.R800026-JLR200
26. Lefebvre P, Cariou B, Lien F, Kuipers F, Staels B. Role of bile acids and bile acid receptors in metabolic regulation. *Physiol Rev*. 2009;89(1):147-191. doi:10.1152/physrev.00010.2008
27. Chiang JYL. Regulation of bile acid synthesis: Pathways, nuclear receptors, and mechanisms. *J Hepatol*. 2004;40(3):539-551. doi:10.1016/j.jhep.2003.11.006
28. Russell DW. THE ENZYMES, REGULATION, AND GENETICS OF BILE ACID SYNTHESIS. 2003. doi:10.1146/annurev.biochem.72.121801.161712
29. Myers RH, Kiely DK, Cupples LA, Kannel WB. Parental history is an independent risk factor for coronary artery disease: The Framingham Study. *Am Heart J*. 1990;120(4):963-969. doi:10.1016/0002-8703(90)90216-K
30. Visscher PM, Wray NR, Zhang Q, et al. 10 Years of GWAS Discovery: Biology, Function, and Translation. *Am J Hum Genet*. 2017;101:5-22. doi:10.1016/j.ajhg.2017.06.005
31. Nikpay M, Beehler K, Valsesia A, et al. Genome-wide identification of circulating-miRNA expression quantitative trait loci reveals the role of several miRNAs in the regulation of cardiometabolic phenotypes. *Cardiovasc Res*.

2019;115(11):1629-1645. doi:10.1093/cvr/cvz030
32. Gebert LFR, MacRae IJ. Regulation of microRNA function in animals. *Nat Rev Mol Cell Biol*. 2019;20(1):21-37. doi:10.1038/s41580-018-0045-7
33. Ge W, Yi M, Pak TR, et al. Overview of MicroRNA Biogenesis, Mechanisms of Actions, and Circulation. *Front Endocrinol | www.frontiersin.org*. 2018;1:402. doi:10.3389/fendo.2018.00402
34. Winter J, Jung S, Keller S, Gregory RI, Diederichs S. Many roads to maturity: MicroRNA biogenesis pathways and their regulation. *Nat Cell Biol*. 2009;11(3):228-234. doi:10.1038/ncb0309-228
35. Catalanotto C, Cogoni C, Zardo G. Molecular Sciences MicroRNA in Control of Gene Expression: An Overview of Nuclear Functions. 2016. doi:10.3390/ijms17101712
36. Bar M, Wyman SK, Fritz BR, et al. MicroRNA Discovery and Profiling in Human Embryonic Stem Cells by Deep Sequencing of Small RNA Libraries. *Stem Cells*. 2008;26(10):2496-2505. doi:10.1634/stemcells.2008-0356
37. Pencheva N, Tran H, Buss C, et al. Convergent multi-miRNA targeting of ApoE grives LRP1/LRP8-dependent melanoma metastasis and angiogenesis. *Cell*. 2012;151(5):1068-1082. doi:10.1016/j.cell.2012.10.028
38. Xia X, Li Y, Wang W, et al. MicroRNA-1908 functions as a glioblastoma oncogene by suppressing PTEN tumor suppressor pathway. *Mol Cancer*. 2015;14(1). doi:10.1186/s12943-015-0423-0
39. Chai Z, Fan H, Li Y, et al. MiR-1908 as a novel prognosis marker of glioma via promoting malignant phenotype and modulating SPRY4/RAF1 axis. *Oncol Rep*. 2017;38(5):2717-2726. doi:10.3892/or.2017.6003
40. Yang L, Shi CM, Chen L, et al. The biological effects of hsa-miR-1908 in human adipocytes. *Mol Biol Rep*. 2015;42(5):927-935. doi:10.1007/s11033-014-3830-1
41. Jiang X, Yang L, Pang L, et al. Expression of obesity-related miR-1908 in human adipocytes is regulated by adipokines, free fatty acids and hormones. *Mol Med Rep*. 2014;10(2):1164-1169. doi:10.3892/mmr.2014.2297
42. Ghanbari M, Sedaghat S, De Looper HWJ, et al. The association of common polymorphisms in miR-196a2 with waist to hip ratio and miR-1908 with serum lipid and glucose. *Obesity*. 2015;23(2):495-503. doi:10.1002/oby.20975
43. Kasai F, Hirayama N, Ozawa M, Satoh · Motonobu, Kohara A. HuH-7 reference genome profile: complex karyotype composed of massive loss of heterozygosity. *Hum Cell*. 2018;31:261-267. doi:10.1007/s13577-018-0212-3
44. Blattmann P, Henriques D, Zimmermann M, et al. Systems Pharmacology Dissection of Cholesterol Regulation Reveals Determinants of Large Pharmacodynamic Variability between Cell Lines. *Cell Syst*. 2017;5(6):604-619.e7. doi:10.1016/j.cels.2017.11.002
45. Mirabelli P, Coppola L, Salvatore M. Cancer cell lines are useful model systems for medical research. *Cancers (Basel)*. 2019;11(8). doi:10.3390/cancers11081098
46. Wessels H-H, Lebedeva S, Hirsekorn A, et al. Global identification of functional microRNA-mRNA interactions in Drosophila. doi:10.1038/s41467-019-09586-z
47. Rogers MA, Liu J, Song BL, Li BL, Chang CCY, Chang TY. Acyl-

CoA:cholesterol acyltransferases (ACATs/SOATs): Enzymes with multiple sterols as substrates and as activators. *J Steroid Biochem Mol Biol*. 2015;151:102-107. doi:10.1016/j.jsbmb.2014.09.008
48. GTEx Portal. https://gtexportal.org/home/snp/rs174561. Accessed January 27, 2020.
49. Kent W, Sugnet C, Furey T, et al. The human genome browser at UCSC. *Genome Res*. 2002;12(6):996-1006.
50. Treiber T, Treiber N, Meister G. Regulation of microRNA biogenesis and its crosstalk with other cellular pathways. *Nat Rev Mol Cell Biol*. 2019;20(1):5-20. doi:10.1038/s41580-018-0059-1
51. Hubbi ME, Semenza GL. Regulation of cell proliferation by hypoxia-inducible factors. *Am J Physiol - Cell Physiol*. 2015;309(12):C775-C782. doi:10.1152/ajpcell.00279.2015
52. Chen Y, Li T, Gao Q, Wang L-Y, Cui L-Q. *MiR-1908 Improves Cardiac Fibrosis after Myocardial Infarction by Targeting TGF-B1*.
53. Agarwal V, Bell GW, Nam JW, Bartel DP. Predicting effective microRNA target sites in mammalian mRNAs. *Elife*. 2015;4(AUGUST2015). doi:10.7554/eLife.05005
54. Riffo-Campos ÁL, Riquelme I, Brebi-Mieville P. Tools for sequence-based miRNA target prediction: What to choose? *Int J Mol Sci*. 2016;17(12). doi:10.3390/ijms17121987
55. Lehrman MA, Schneider WJ, Südhof TC, Brown MS, Goldstein JL, Russell DW. Mutation in LDL receptor: Alu-Alu recombination deletes exons encoding transmembrane and cytoplasmic domains. *Science (80-)*. 1985;227(4683):140-146. doi:10.1126/science.3155573
56. Banerjee S, Andrew RJ, Duff CJ, et al. proteolysis of the low density lipoprotein receptor by bone morphogenetic protein-1 regulates cellular cholesterol uptake. doi:10.1038/s41598-019-47814-0
57. Strøm TB, Bjune K, Leren TP. Bone morphogenetic protein 1 cleaves the linker region between ligand-binding repeats 4 and 5 of the LDL receptor and makes the LDL receptor non-functional. *Hum Mol Genet*. October 2019. doi:10.1093/hmg/ddz238
58. miRIDIAN microRNA Mimic. https://horizondiscovery.com/products/gene-modulation/knockdown-reagents/mirna/PIFs/miRIDIAN-microRNA-Mimic?nodeid=mirnaprecursor-mi0008329. Accessed January 27, 2020.
59. Garzon R, Marcucci G, Croce CM. Targeting microRNAs in cancer: Rationale, strategies and challenges. *Nat Rev Drug Discov*. 2010;9(10):775-789. doi:10.1038/nrd3179
60. Shah MY, Ferrajoli A, Sood AK, Lopez-Berestein G, Calin GA. microRNA Therapeutics in Cancer — An Emerging Concept. *EBioMedicine*. 2016;12:34-42. doi:10.1016/j.ebiom.2016.09.017

Appendix A- Supplementary Figures

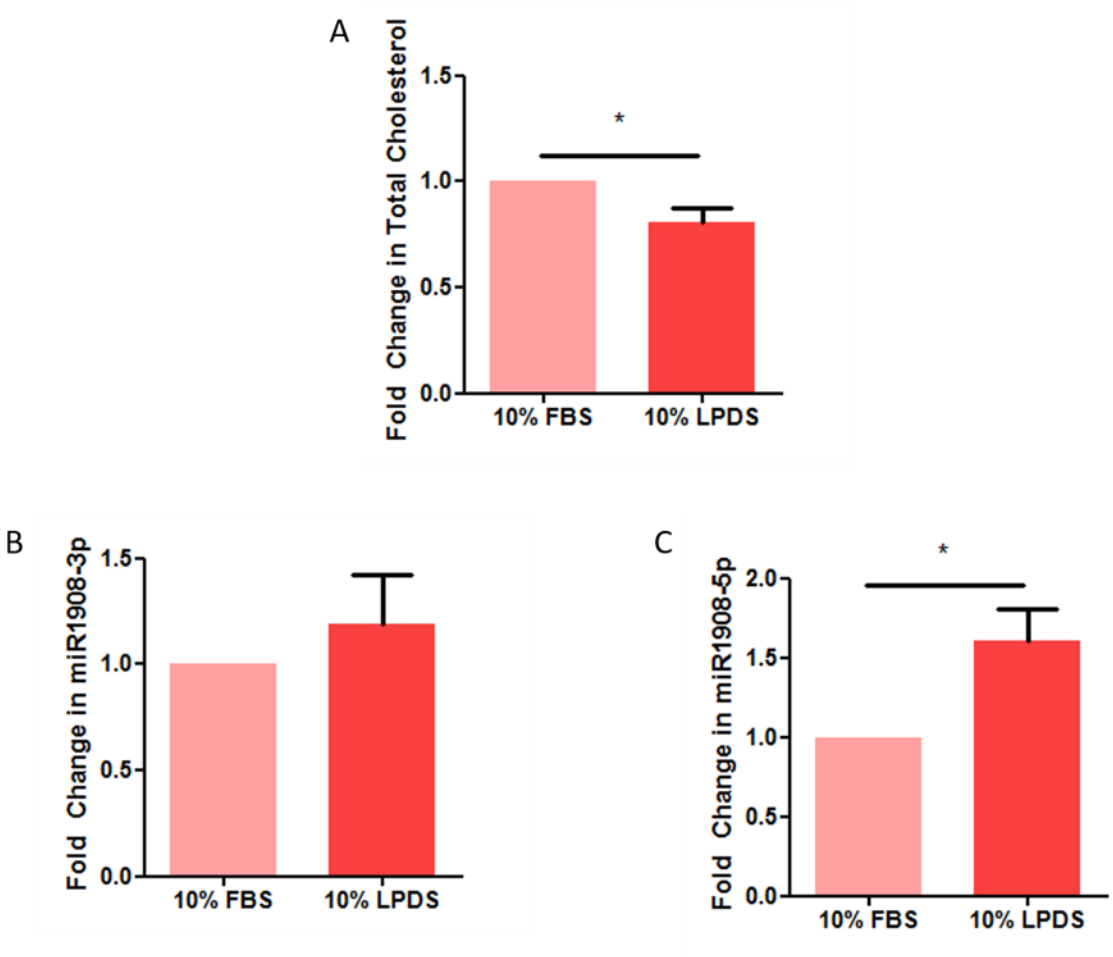

Figure S1. miR-1908-5p expression increases in LPDS medium.
HuH-7 cells were placed in 10% LPDS medium for 72 hours followed by RNA and lipid extraction. (A) The total cholesterol concentration, normalized to protein concentration, was calculated relative to untreated cell in 10% FBS medium using the Amplex Red Cholesterol Assay. QRT-PCR was performed to measure the fold change in (B) miR-1908-3p or (C) miR-1908-5p relative to the untreated cells, using miR-16 and RNU48 for normalization. N=4. The error bars depict the SD. *p<0.05.

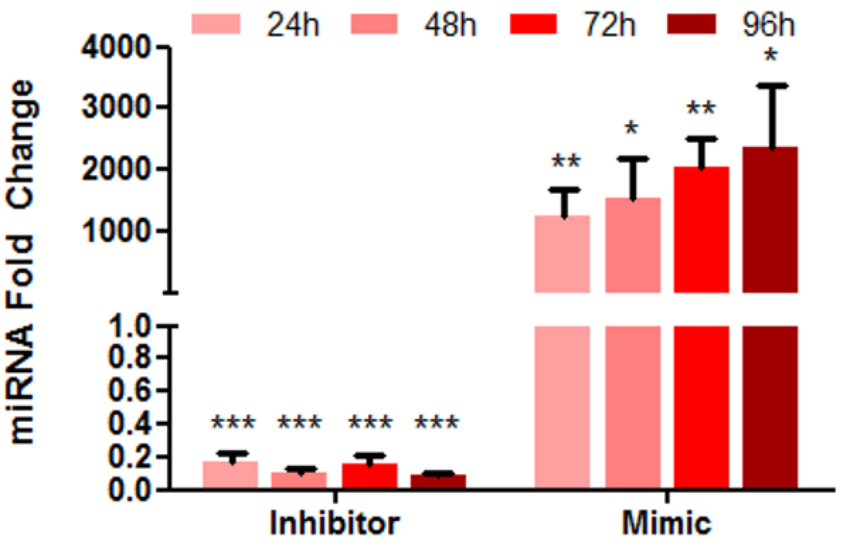

Figure S2. Validation of the miR-1908-5p inhibitor and mimic in HuH-7 cells.
HuH-7 cells were treated with 9 nM of miR-1908-5p inhibitor, mimic, or transfection control for 24, 48, 72, and 96 hours. The expression of miR-1908-5p was analyzed using qRT-PCR. The mean fold change was calculated relative to the transfection control using miR-16 and RNU48 for normalization. N=3. The error bars depict the SD. *p<0.05, **p<0.01, ***p<0.001.

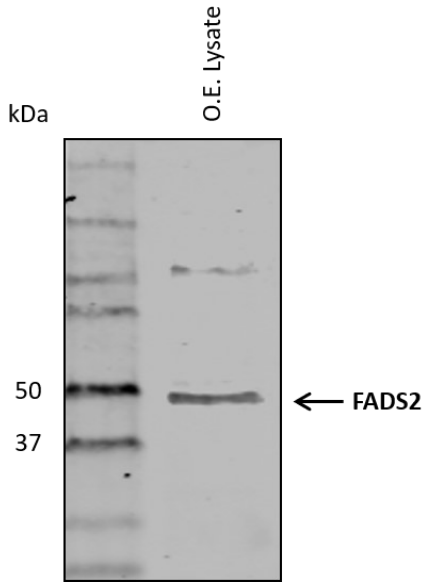

Figure S3. Western blot positive control for FADS2.
20 µg of the FADS2 Human Over-expression Lysate (OriGene) was run on a western blot and a rabbit polyclonal antibody (GeneTex) was used to detect FADS2.

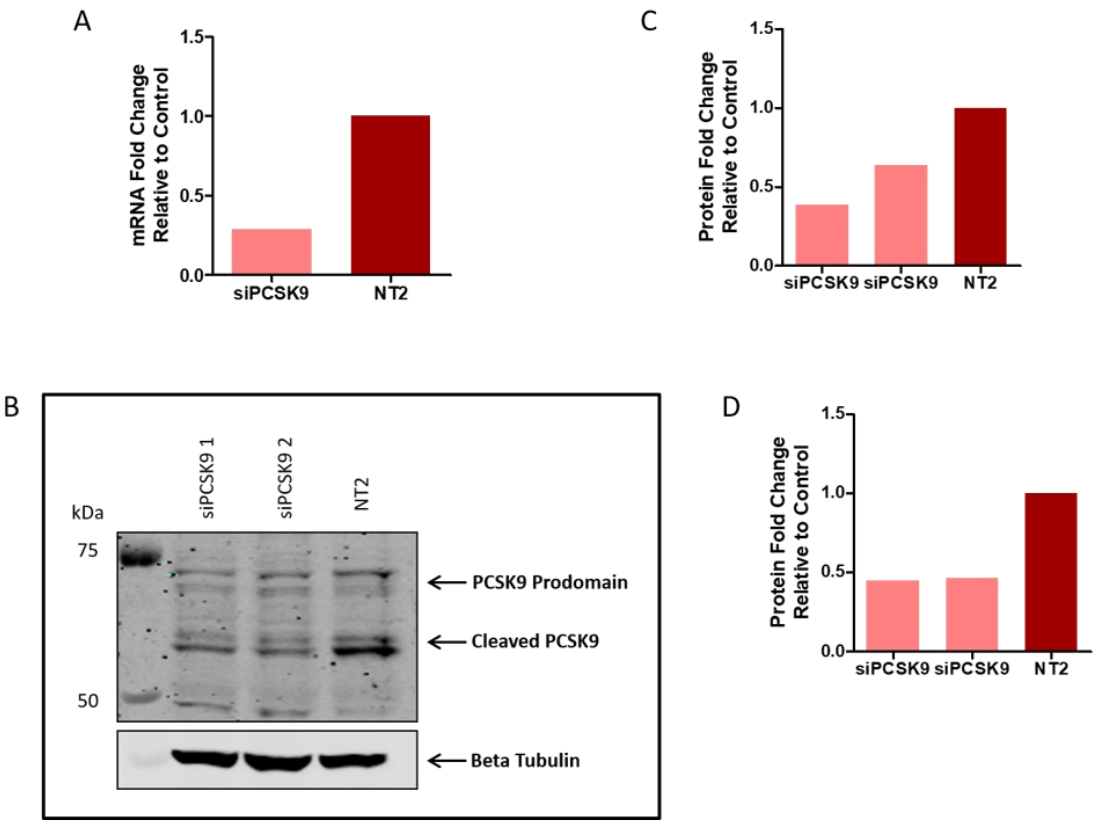

Figure S4. Successful knockdown of PCSK9 for western blot validation. Huh7 cells were treated for 48 hours with 20nM siRNA targeting *PCSK9*. (A) The mRNA expression was analyzed using qRT-PCR. The fold change was calculated relative to the non-target control using *HPRT1* and *SRP14* for normalization. (B) A Western blot was performed using Beta tubulin as a loading control to measure the fold change in (C) the PCSK9 prodomain and (D) the cleaved PCSK9 expression relative to the non-target control.

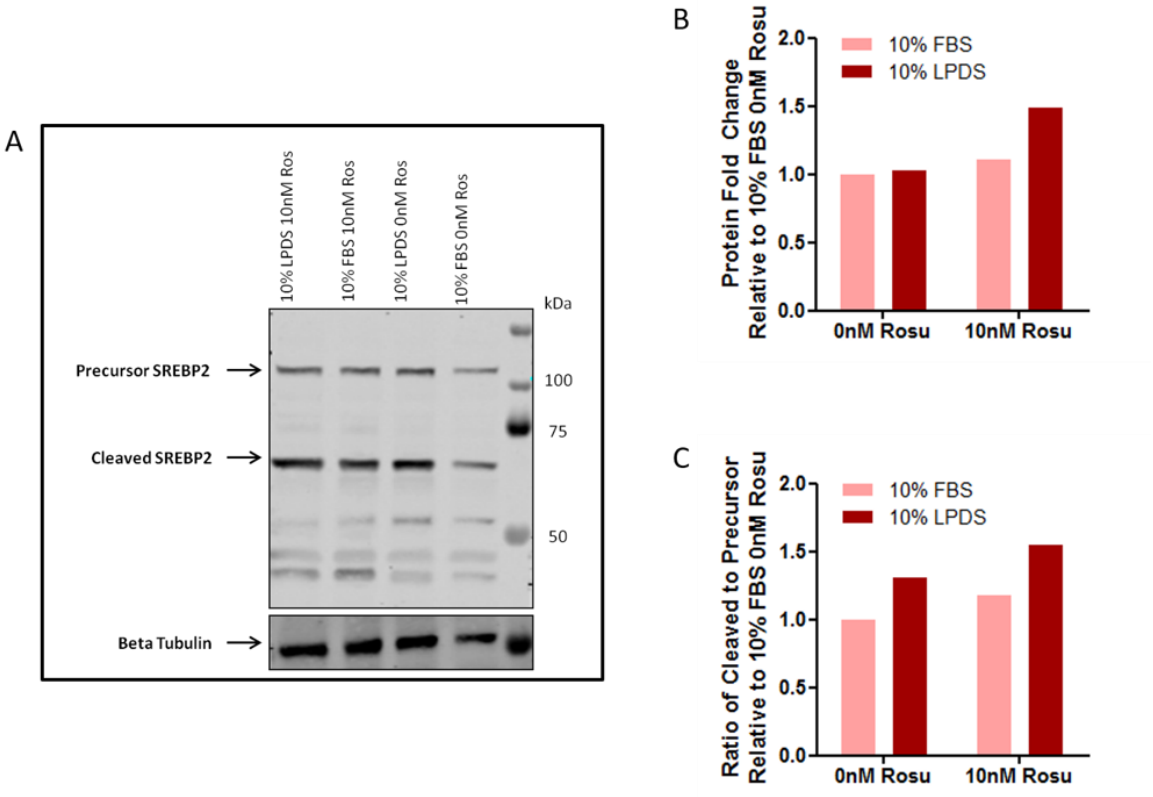

Figure S5. SREBP2 expression increases under cellular cholesterol depletion conditions.
HuH-7 cells were treated with 10 nM rosuvastatin (Rosu) in medium containing 10% FBS or 10% LPDS. After 72 hours, the protein was extracted from the cells and (A) a Western blot was performed to detect SREBP2. Beta tubulin was used as a loading control to measure the fold change in (B) total SREBP2 expression and (C) the ratio of cleaved to precursor SREBP2 expression relative to the untreated cells.

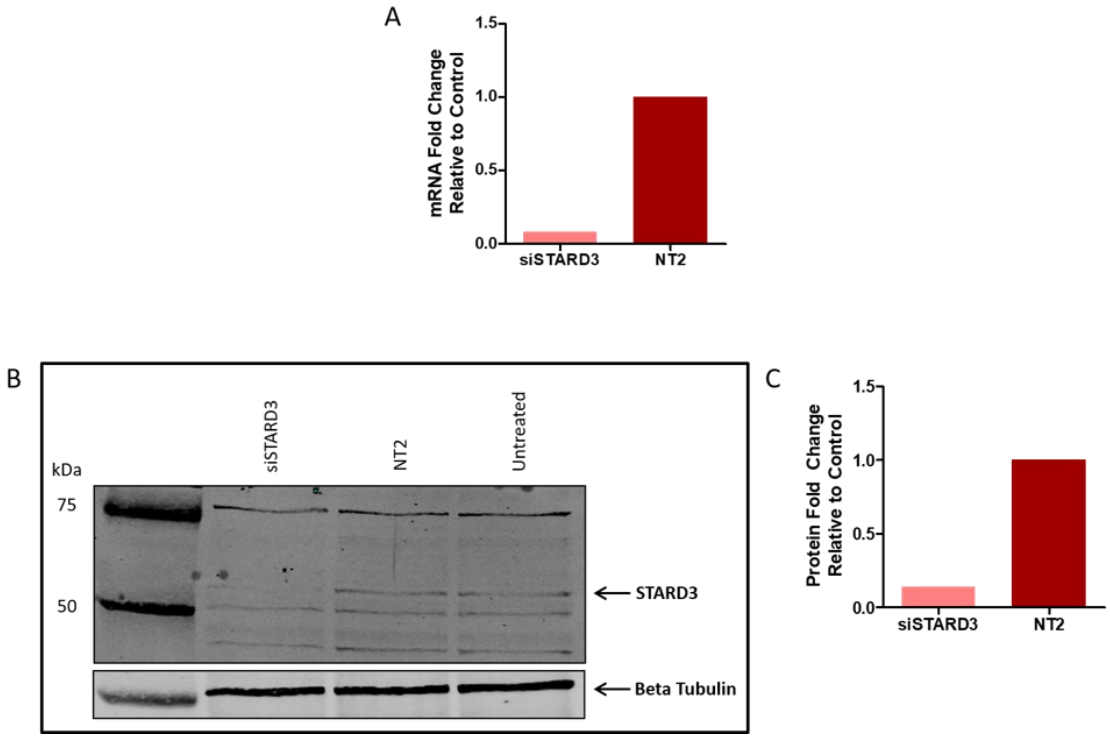

Figure S6. Successful knockdown of STARD3 for western blot validation. Huh7 cells were treated for 48 hours with 20nM siRNA targeting *STARD3*. (A) The mRNA expression was analyzed using qRT-PCR. The fold change was calculated relative to the non-target control using *HPRT1* and *SRP14* for normalization. (B) A Western blot was performed using Beta tubulin as a loading control to measure the fold change in (C) STARD3 protein expression relative to the non-target control.

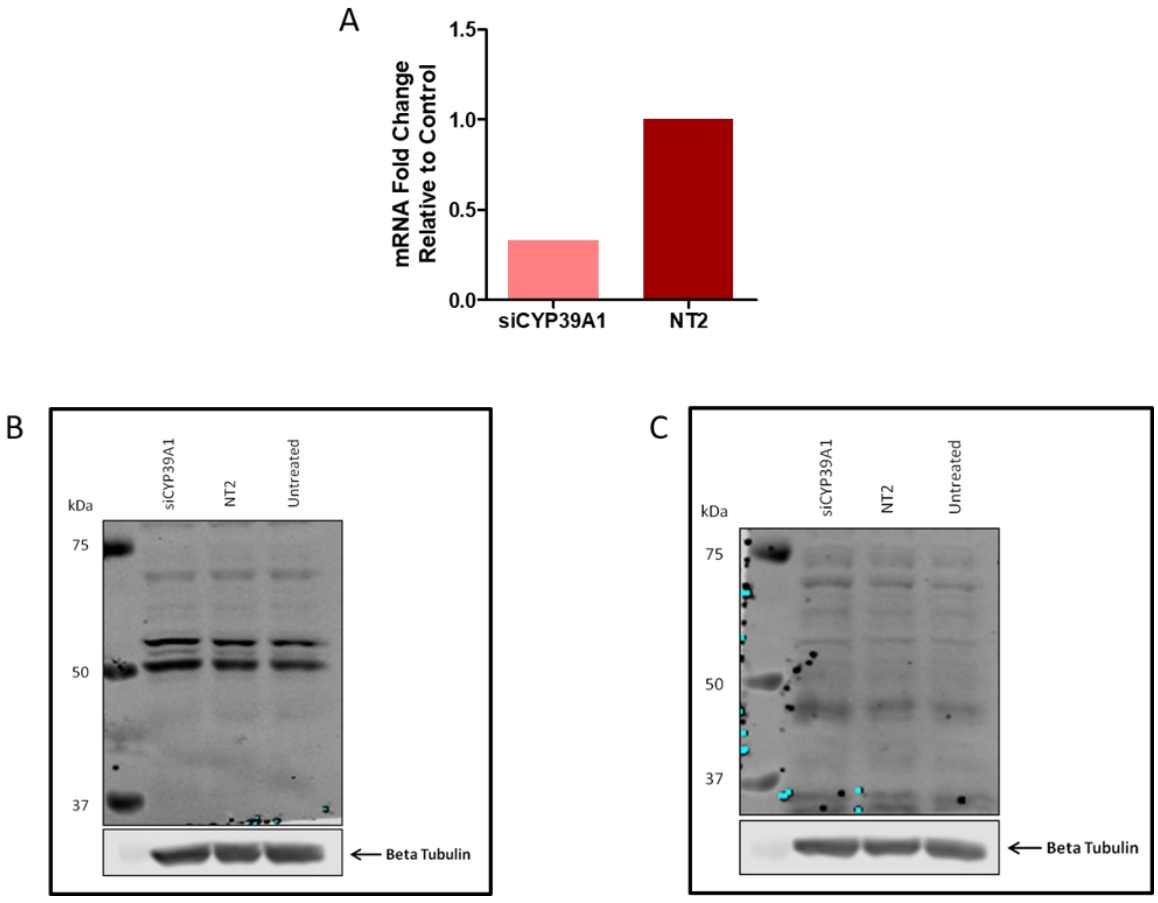

Figure S7. Successful knockdown of *CYP39A1* RNA is undetectable at the protein level.
Huh7 cells were treated for 48 hours with 20nM siRNA targeting *CYP39A1*. (A) The mRNA expression was analyzed using qRT-PCR. The fold change was calculated relative to the non-target control using *HPRT1* and *SRP14* for normalization. A Western blot was performed using a rabbit polyclonal antibody (B) and a mouse monoclonal antibody (C) to detect CYP39A1. Detection of CYP39A1 was inconsistent between these blots.

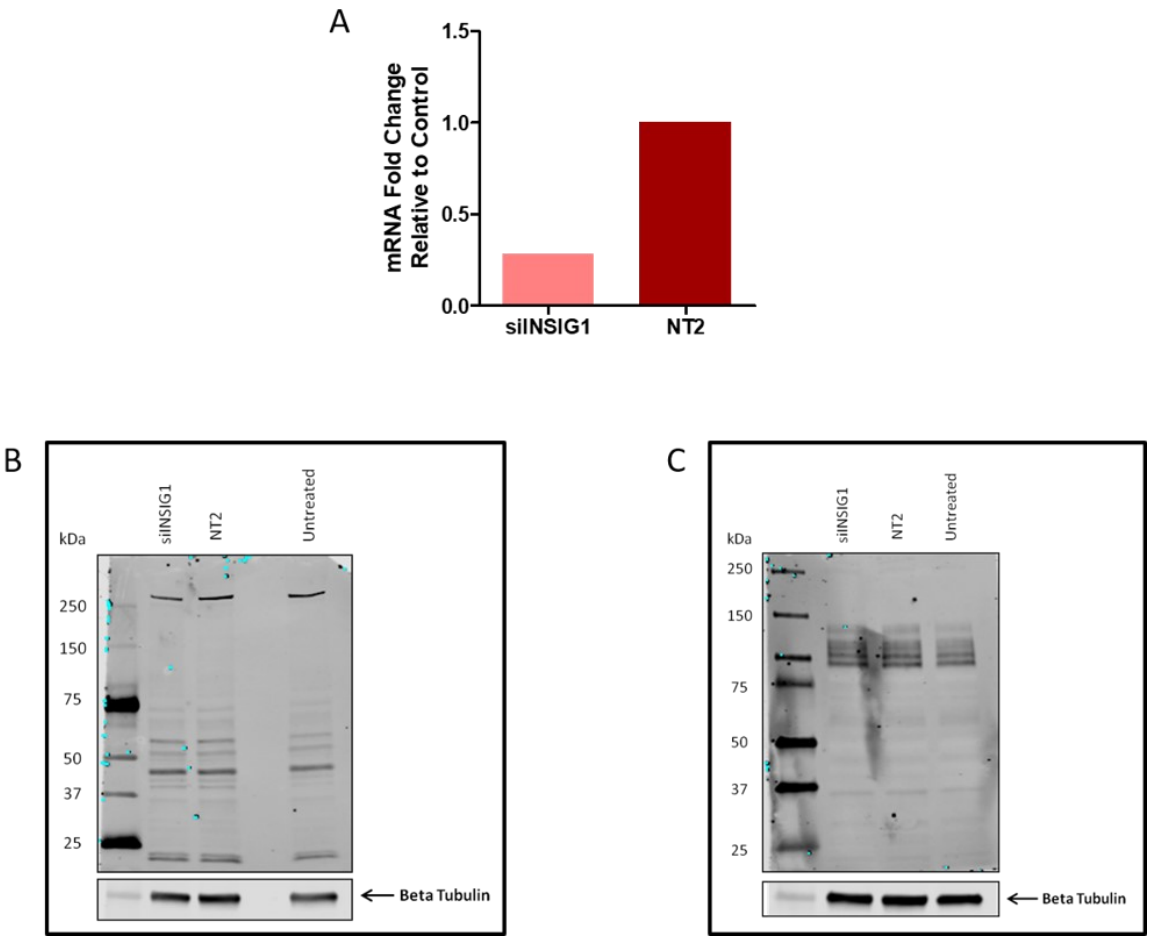

Figure S8. Successful knockdown of *INSIG1* RNA is undetectable at the protein level.
Huh7 cells were treated for 48 hours with 20nM siRNA targeting *INSIG1*. (A) The mRNA expression was analyzed using qRT-PCR. The fold change was calculated relative to the non-target control using *HPRT1* and *SRP14* for normalization. A Western blot was performed using a rabbit polyclonal antibody from Abcam (B) or from Novus (C) to detect INSIG1. Detection of INSIG1 was inconsistent between these blots.

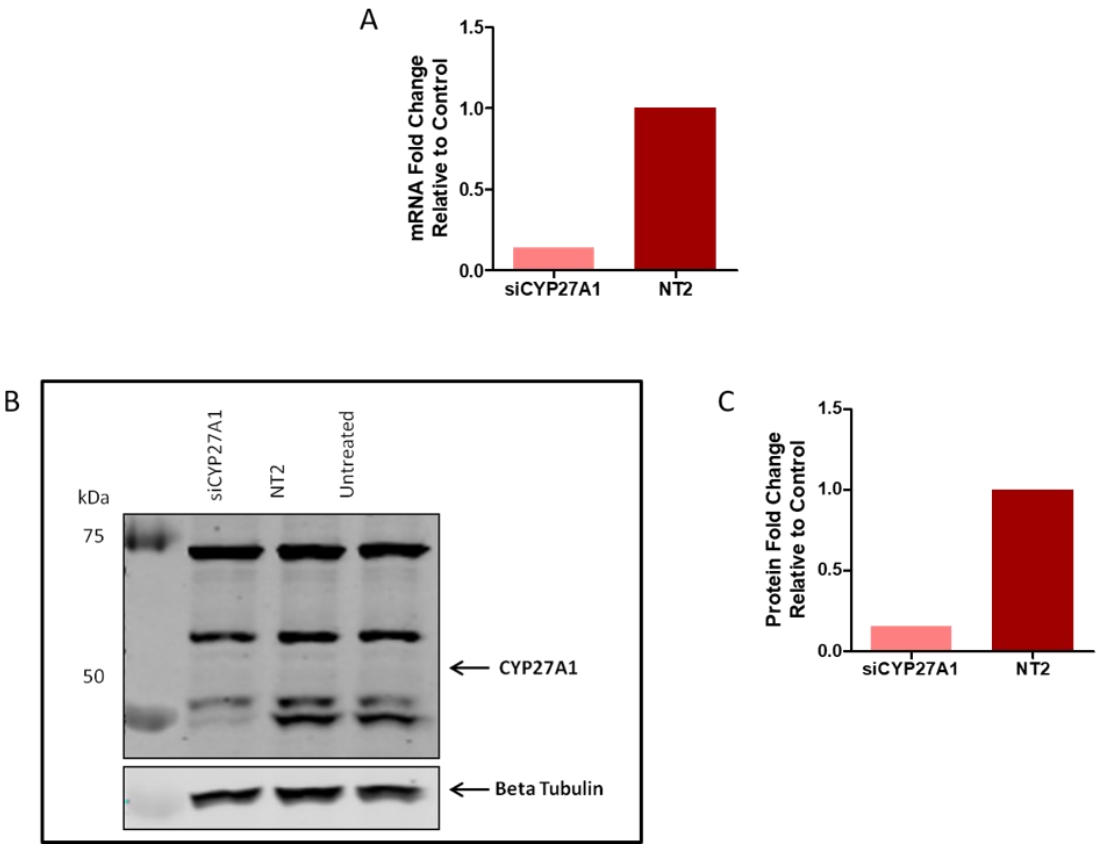

Figure S9. Successful knockdown of CYP27A1 for western blot validation. Huh7 cells were treated for 48 hours with 20nM siRNA targeting *CYP27A1*. (A) The mRNA expression was analyzed using qRT-PCR. The fold change was calculated relative to the non-target control using *HPRT1* and *SRP14* for normalization. (B) A Western blot was performed using Beta tubulin as a loading control to measure (C) the fold change in CYP27A1 protein expression relative to the non-target control.

Appendix B- Curriculum Vitae

Kaitlyn Beehler

Profile

I am a highly determined and focused MSc candidate with valuable knowledge in molecular biology. I have demonstrated success in my abilities to design, conduct, and analyze experimental data. I have developed meticulous and strategic experimental intelligence that promotes accuracy and authentication. I am driven to succeed in the science industry with my impeccable time management skills, my remarkable presentation competence and my ability to adapt in ever-changing situations.

Education

University of Ottawa **2018-2020**
Masters of Science Biochemistry

University of Ottawa **2014-2018**
Honours Bachelor of Science in Biochemistry Option in Microbiology and Immunology

Educational Achievements

- Admission scholarship-Masters, University of Ottawa- 2018
- Graduated with Cum Laude, University of Ottawa – 2014-2018
- Dean's Honours List, University of Ottawa – 2017-2018

Experience

Masters of Biochemistry Student **2018-2020**
Atherogenomics Laboratory, Dr. Ruth McPherson
The University of Ottawa Heart Institute, Ottawa, Ontario

miR-1908 is a cholesterol responsive microRNA implicated in cholesterol regulation

- Reviewed scientific literature before designing, conducting, and analyzing complex experiments
- Manipulated, maintained, and transfected immortal cell lines
- Used cholesterol assays to show that miR-1908-5p expression is dependent on cellular cholesterol levels

- Used qRT-PCR and western blots to validate targets of miR-1908-5p related to cholesterol metabolism
- Trained and supervised students

Honours Project Student **2017-2018**
Atherogenomics Laboratory, Dr. Ruth McPherson
The University of Ottawa Heart Institute, Ottawa, Ontario

Analysis of microRNA-133a/b inhibition on brown adipogenesis in human skeletal muscle precursor cells

- Reviewed scientific literature before designing, conducting, and analyzing complex experiments
- Manipulated and maintained primary cell lines
- Performed cell staining using Oil Red O
- Extracted RNA and microRNA from cells using various techniques followed by qRT-PCR
- Wrote a scientific manuscript

Research Assistant **2016-2018**
Atherogenomics Laboratory, Dr. Ruth McPherson
University of Ottawa Heart Institute, Ottawa, ON

- Aided in the determination of a functional polymorphism in the *SGCG* gene highly expressed in skeletal muscle cells that associates with the capacity for weight loss in response to energy restriction
- Manipulated and maintained immortal and primary cell lines
- Cloned and generated Lenti-virus to use as a gene delivery tool for primary culture cells
- Performed Luciferase assays on culture cells to determined fold changes in promoter/enhancer activity across different treatments
- Extracted DNA and RNA from whole human blood and cell lines using a variety of techniques
- Mastered molecular biology techniques: cloning, transformation, transfection, PCR, and Quantitative Real-time RT-PCR
- Characterized and quantified proteins using BCA assays and western blotting
- Created, executed, and updated complex protocols
- Trained and supervised students

Sales Associate and Designer **2008-2019**
Meadow Greens Nursery, Russell, ON

- Designed flower gardens and planters based on customers' preferences
- Created merchandise displays within the greenhouse

- Transplanted and cared for many different types of plants
- Provided customer service by working the cash, giving advice on flowers, and answering the phone

Skills

- Proficient in conducting scientific literature searches
- Confident in writing reports and presenting research in various ways (posters, presentations etc.)
- Extensive knowledge of qRT-PCR, western blotting, and cholesterol assays
- Capable of troubleshooting experimental shortcomings
- Software and computational tools: Microsoft Word, Excel, Powerpoint, GraphPad Prism, UCSC genome browser, Blast, primer design and various scientific analysis software

Volunteer Experience

Work in Progress (WIP) Coordinator **2019-2020**
University of Ottawa Heart Institute Trainee Committee

- Attended monthly meetings to discuss concerns and ideas brought forth by trainees and to brainstorm ideas to promote trainee involvement in Heart Institute organized events
- Schedule, moderate, and advertise weekly work in progress rounds at the Heart Institute to give trainees the opportunity to present their research and promote cross-disciplinary collaborations

Let's Talk Science Volunteer **2018-2020**
University of Ottawa

- Lead elementary and high school students through hands-on STEM activities and demonstrations in the classroom
- Explain difficult concepts from their science curriculum in a comprehendible and fun way

Publications and Papers

Beehler K. miR-1908 is a cholesterol responsive microRNA implicated in cholesterol regulation. Department of Biochemistry, Microbiology and Immunology, University of Ottawa. MSc. Thesis. 2020

Nikpay M., **Beehler K**., Valsesia A., et al. Genome-wide identification of circulating-miRNA expression quantitative trait loci reveals the role of several miRNAs in the regulation nof cardiometabolic phenotypes. *Cardiovascular Res.* 2019; 115(11): 1629-1645. Doi: 10.1093/cvr/cvz030

Beehler K. Analysis of microRNA-133a/b inhibition on brown adipogenesis in human skeletal muscle precursor cells. Department of Biochemistry, University of Ottawa. Honours Thesis. 2018.

Presentations and Abstracts

Beehler K., Nikpay M., Lau P., Soubeyrand S., McPherson R. The role of GWAS identified miR-1908 in hepatic cholesterol regulation. University of Ottawa Heart Institute Trainee Committee Work in Progress Rounds. Oral Presentation. Ottawa, Ontario. December 2019.

Beehler K., Nikpay M., Lau P., Soubeyrand S., McPherson R. miR-1908 is a cholesterol responsive microRNA Implicated in LDL Receptor maturation. Canadian Vascular & Lipid Summit. Poster presentation. Banff, Alberta. October 2019.

Beehler K., Lau P., Soubeyrand S., Nikpay M., McPherson R. The role of miR-1908-5p on cholesterol metabolism. University of Ottawa BMI Poster Day. Poster Presentation. Ottawa, Ontario. May 2019.

Beehler K., Lau P., Soubeyrand S., Nikpay M., McPherson R. The role of miR-1908-5p on cholesterol metabolism. University of Ottawa Heart Institute Annual Research Day. Poster Presentation. Ottawa, Ontario. May 2019.